ADVANCED THERAPEUTICS
www.advtherap.com

Hiltonol, a dsRNA Mimic, Promotes NK Cell Anticancer Cytotoxicity Through TAZ Cytoplasmic Sequestration

*Darren Chen Pei Wong, Zekun Xia, Nandi Shao, Ivan Yow, T. Thivakar, Jin Ye Yeo, Andres M. Salazar, Yih-Cherng Liou, Boon Chuan Low, and Jeak Ling Ding**

The evolutionarily conserved YAP/TAZ mechanoresponsive transcription cofactors regulate development and tumorigenesis. Here, it is shown for the first time that human natural killer (NK) cells specifically express TAZ but not YAP, and TAZ serves to limit NK cytotoxicity. The synthetic double-stranded RNA, hiltonol, is able to trigger cytoplasmic compartmentalization of TAZ, which increases NK cytotoxicity. Mechanistically, a low dose of hiltonol enhances the actin-based intracellular contractility of NK cells accompanied by an increase in active RhoA and myosin light chain phosphorylation, conceivably through an increase in ERK1/2 activation-dependent ROS production. Importantly, it is showed that the dissociation of LATS1 from actin upon activation of contractility is associated with TAZ cytoplasmic localization. Functionally, hiltonol also reduces the NK cell surface inhibitory receptors, e.g., KIR3DL1, through c-Myc inhibition. Direct inhibition of c-Myc promotes NK cytotoxicity against K562 lymphoblast. The findings are corroborated by coculturing hiltonol-pretreated NK cells with breast and lung cancer cells, and increased NK-mediated cancer killing is demonstrated, which conceivably occurs via compartmentalization of TAZ to the cytoplasm which facilitates NK cytotoxicity. The findings pave the way for ex vivo rejuvenation of NK cells for in vivo immunotherapies, which can involve a cocktail of low dose hiltonol and c-Myc inhibitor.

1. Introduction

The innate immune natural killer (NK) cells are indispensable in defending against infection and cancer.[1–4] Of particular interest is the integration of intrinsic and extrinsic cell and molecular, biochemical, and biophysical signals, which activate dormant transcriptional networks responsible for NK cytotoxicity through various pattern recognition receptors (PRRs), for example, Toll-like receptors (TLRs) 1–9 in humans.[5–8] Upon activation, NK cells elicit their cytolytic capabilities mainly through the production of granzyme and perforin, followed by degranulation of these effectors to cytolyze target cells. Like other immune cells, NK cell activation has traditionally been associated with the integration of activating and inhibitory signals through several activating (e.g., NKG2D and DNAM-1) and inhibitory (e.g., PD-1, KIR family receptors, and TIGIT) cell surface receptors.[2,9,10] However, several key questions remain on how the advanced stages of cancer cells evade these activating signals, through downregulation of NK cell cytotoxicity or promotion of NK cell exhaustion. Importantly, what are the extrinsic and intrinsic triggers that modulate NK cell activity to reinvigorate it for cancer immunotherapy? We have recently identified intracellular contractility in NK cells, which upregulates NK cytotoxicity by promoting nuclear localization of transcription factor, Eomes.[1] Other studies also suggested that NK cells respond to mechanical forces,[11] indicating that increased

D. C. P. Wong, Z. Xia, N. Shao, J. Y. Yeo, Y.-C. Liou, B. C. Low, J. L. Ding
Department of Biological Sciences
National University of Singapore
Singapore 117543, Singapore
E-mail: dbsdjl@nus.edu.sg

The ORCID identification number(s) for the author(s) of this article can be found under https://doi.org/10.1002/adtp.202300016

DOI: 10.1002/adtp.202300016

D. C. P. Wong, I. Yow, T. Thivakar, B. C. Low
Mechanobiology Institute Singapore
National University of Singapore
Singapore 117411, Singapore

A. M. Salazar
Oncovir Inc
3203 Cleveland Avenue Northwest Washington, DC 20008, USA

B. C. Low
NUS College
National University of Singapore
Singapore 138593, Singapore

J. L. Ding
Integrative Sciences and Engineering Programme
National University of Singapore
Singapore 119077, Singapore

substrate stiffness enhances NK cell cytotoxicity.[12,13] However, it is well known that cancer cells are softer than normal cells, especially for highly metastatic cancer cells.[14,15] Hence, it is of interest to delineate mechanosensitive pathways that can bypass or pre-empt cancer cell softening and enhance NK cytotoxicity for potential therapeutic options.

Poly-ICLC (Hiltonol) is an advanced form of the synthetic poly-I:C dsRNA derivative stabilized with poly-lysine and carboxymethyl cellulose that effectively enters the endosome, thus making it a "reliable and authentic" viral mimic that activates the human PRRs (e.g., TLR3 and MDA-5).[16] NK cells recognize dsRNA, a viral replication intermediate, and mediates proinflammatory responses through type I interferons and chemokines.[8,17,18] However, recent studies suggest that upon stimulation by dsRNA, NK cells can induce dendritic cell maturation[8] and activation of NK cell TLR3 induces NK-cancer killing activity. Several clinical trials using dsRNA as an adjuvant for therapeutic vaccination against cancers are also underway.[19,20] Despite extensive studies on the role of dsRNA mimics in inducing immune responses through inflammation, the mechanisms underlying dsRNA-induced NK cytotoxicity has remained unclear. Interestingly several conflicting studies implicate the role of TLRs in regulating cellular contractility in aortic vascular smooth muscle cells and cardiomyocytes.[21,22] To seek clarity and to fill the knowledge gap, a study of contractility and mechanosensitive pathways regulated by NK contractility is pertinent and essential. Moreover, the important, yet variegated roles of the cytoskeleton in NK cell are increasingly gaining attention.[11,23–27]

Various NK cell immunodeficiency diseases are purportedly caused by the misregulation of cytoskeletal proteins.[28] We have previously shown that despite lacking focal adhesions, NK cells can remarkably alter intracellular contractility for nuclear localization of the transcription factor, Eomes, and elicit early cytotoxic responses against cancer cells.[1] Furthermore, biochemical and biophysical signals should be integrated to regulate pathophysiological activities. For instance, the Hippo-Yes-associated protein (YAP)/WW domain-containing transcription regulator 1 (WWTR1, commonly referred to as TAZ) pathway is biochemically and biophysically coregulated.[29–31]

The Hippo-YAP/TAZ pathway was first identified as a growth regulator and its dysregulation was reported to promote tumorigenesis.[30,32] YAP and TAZ are transcription cofactors that are canonically inhibited by the Hippo pathway through a series of kinases (MST and LATS) which are sequentially activated by phosphorylation.[31,33] Recent findings suggest that YAP and TAZ are mechanoresponsive, and their subcellular compartmentalization can be affected by mechanical forces.[34] However, the mechanistic roles of Hippo-YAP/TAZ in immune cells have hitherto remained unclear. Recent evidence suggests that YAP suppresses CD8 T-cell differentiation and function.[35] However, how and whether Hippo-YAP/TAZ affects NK cell activity, needs clarification. Moreover, the triggers and mechanisms that activate or inactivate the Hippo pathway to regulate YAP/TAZ activity in NK cells are unknown. Since TLR3 activation was shown to induce endothelial cell contractility[22] and YAP/TAZ are mechanoregulated,[30,36] it is possible that NK cell contractility can control YAP/TAZ through mechanotransduction events. This prompted us to hypothesise that TLR3 activation regulates YAP/TAZ subcellular localization through enhanced NK cell contractility, which potentially modulates NK cytotoxicity.

Here, using primary human NK (hNK) cells and an NK cell line undergoing clinical trial (NK-92), we show that NK cells uniquely express TAZ but not YAP mRNA and protein. Overexpression and knockdown of TAZ suppressed and enhanced NK cell cytotoxicity, respectively, suggesting that inhibition of TAZ could heighten NK cytotoxicity. Next, we showed that treatment of NK cells with TLR3 agonist, hiltonol, promoted the cytoplasmic compartmentalization of TAZ, which was associated with increased NK cytotoxicity. We used multimodal approaches to provide mechanistic evidence for hiltonol-mediated activation of ERK1/2, which enhanced intracellular contractility. This was demonstrated by an increase in F-actin tensional force in laser ablation experiments and an increase in RhoA-MLC2 activation. Our results showed that i) activated ERK1/2 raised the mitochondrial ROS level, ii) enhanced NK contractility released LATS1 kinase from actin which correlated with LATS1 phosphorylation at Ser89, and iii) phosphorylated LATS1 then phosphorylated and inhibited TAZ, which became sequestered in the cytoplasm. We also identified c-Myc, a known downstream target of TAZ activation,[37] to conversely limit NK cytotoxicity and found that in the presence of nuclear TAZ, c-Myc activity maintained a high level of inhibitory receptor, KIR3DL1, on NK cells. On the other hand, the inhibition of c-Myc directly or through hiltonol treatment, reduced NK inhibitory receptor to unleash the cytotoxic potential of NK cells against cancer cells. Taken together, we have demonstrated, in a lymphoblast cell line and two cancer cell types (breast and lung), that hiltonol treatment increased NK cell cytotoxicity against cancer cells. Our findings provide potentials for immunomodulating NK cells to kill cancers.

2. Results

2.1. TAZ Knockdown Enhances NK Cell Cytotoxicity

Since YAP and TAZ are homologs with similar structure and function,[29,30] we first verified if YAP and TAZ are equally expressed in NK cells. Surprisingly, we could only detect TAZ but not YAP expression at both the mRNA (**Figure 1**A) and protein (Figure 1B) levels in both NK-92 and primary hNK cells. Upon cross referencing with the available online database,[38] we confirmed that indeed NK cells only expressed TAZ but not YAP (Figure S1, Supporting Information).

Being homologous, YAP and TAZ are apparently regulated by similar mechanisms in various systems.[30,31] Since YAP has been reported to elicit a broad inhibitory role in T cells (CD4 and CD8),[33,35,36,39] which are of the common lymphoid lineage including innate NK cells, we hypothesized that TAZ might also regulate NK cytotoxicity. To test this, we performed siRNA knockdown of TAZ in NK-92 cells (Figure 1C,D). We observed significant upregulation of key cytotoxic molecules (granzyme B and perforin) in TAZ-knocked down NK-92 cells as indicated by flow cytometric analysis (Figure 1E). These results are indicative of a general increase in NK-92 cytotoxicity. Interestingly, the proliferation rate of NK-92 cells, as indicated by Ki67, remained unchanged when comparing TAZ-knocked down NK-92 to control siRNA or wild type NK-92 cells (Figure 1F). Nevertheless, the viability of NK-92 cells also remained unchanged after knock-

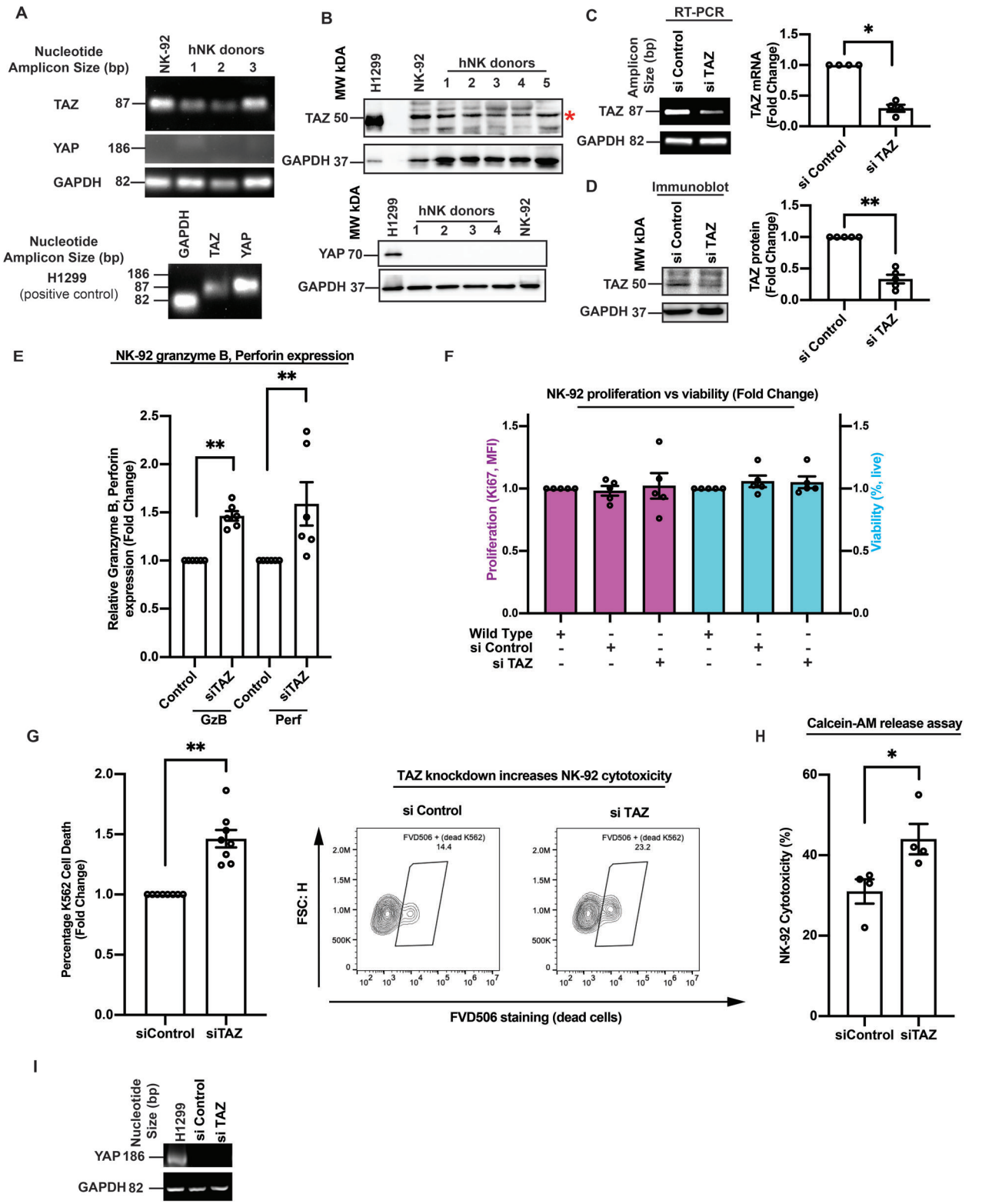

Figure 1. TAZ knockdown enhances NK cell cytotoxicity in vitro. A) RT-PCR analysis shows that NK-92 cell line and three primary human NK (hNK) cells from healthy donors express TAZ but not YAP. The H1299 NSCLC cells (positive control) express both TAZ and YAP. All RT-PCR analyses were repeated thrice, and a representative gel blot was shown. The size markers represent the nucleotide amplicon size and not gene size. B) Immunoblot shows NK-92 and hNK cells express TAZ protein but not YAP protein. H1299 NSCLC was used as a positive control. All blots were repeated thrice, and a representative image was shown. C,D) RT-PCR and immunoblot analyses show knockdown of mRNA and protein levels in NK-92 cells treated with TAZ siRNA. Note the size markers for RT-PCR images represent the nucleotide amplicon size and not gene size. Quantification of the results are represented

down of TAZ. To ascertain the functionality of NK-92 cells after knockdown of TAZ, we performed a killing assay using the Fixable Viability Dye eFluor 506 dye that irreversibly labels dead cells (Fvd506 positive, see Figure S2 of the Supporting Information for gating strategy) and can be fixed and washed to stain for intracellular antigens without any loss of staining intensity of the dead cells.[1,40] The CellTrace Far Red-stained myelogenous leukemia K562 model cell line was stained with Fvd506 dye after coculturing with NK-92 cells for 4 h and NK-92 TAZ-knocked down cells demonstrated enhanced killing efficiency against K562 cells (Figure 1G). To account for the possibility that CellTrace Far Red could also stain NK-92 cells resulting in an over/underestimation of NK cytotoxicity due to NK-92 spontaneous cell death, we performed a Calcein-AM release assay to quantify released calcein in the culture medium after coculturing Calcein-AM-labeled K562 target cells with NK-92 cells. Indeed, TAZ knockdown specifically increased NK-92 cytotoxicity against K562 cells (Figure 1H). Since several studies implicated YAP in dampening T cell responses,[33,35,36,39] we also performed an RT-PCR of YAP expression in TAZ-knocked down NK-92 cells. As shown in Figure 1I, the loss of TAZ was not compensated for by YAP expression.

Together, our results showed that NK cells express TAZ but not YAP, and TAZ knockdown enhances NK-92 cytotoxicity. Since TAZ is a transcriptional coactivator, we reasoned that understanding the conditions that influence TAZ modulation, for example its subcellular compartmentalization would be mechanistically enlightening. Henceforth, we focused on possible factors altering TAZ subcellular localization in NK cells.

2.2. dsRNA Mimic, Hiltonol, Induces Cytoplasmic Compartmentalization of TAZ and Increases NK Cytotoxicity

Although first identified to be an antiviral receptor responding to viral dsRNA[8,20] recent studies suggest that dsRNA activation in NK cells (e.g., through TLR3) elicit cytotoxic effects on cancer.[8,17,41] Other studies also demonstrated that TLR3 activates cellular contractility in nonimmune systems.[18,21,22] Since YAP/TAZ are mechanosensitive and TLR3 has potential antitumor capabilities, we reasoned that activation of TLR3 by hiltonol might regulate the subcellular localization of TAZ.

To test whether hiltonol treatment likely activates TLR3 pathways, we treated hNK cells with hiltonol and observed a significant dose-dependent increase in TLR3 expression in hiltonol-treated hNK cells (Figure S3A, Supporting Information). Confocal images of TAZ localization showed that hiltonol induced a significant cytoplasmic sequestration of TAZ, corresponding to the dose of hiltonol, in both NK-92 (**Figure 2**A) and hNK cells (Figure 2B), but without affecting cell viability (Figure S3B, Supporting Information). Interestingly, in control resting NK cells, TAZ was homogeneously present in both the cytoplasm and nucleus of NK cells, in contrast to being predominantly present in the nucleus of adherent cell types.[42,43] To corroborate our observations, we treated NK-92 and hNK cells with hiltonol and performed imaging flow analysis to empirically quantify the overlap signal of nuclear stain (DAPI) to TAZ (Figure 2C–F). In hiltonol-treated NK cells, we quantified lesser overlap in nuclear signal of TAZ (represented by median similarity TAZ/DAPI score) at a level which was consistent with the cytoplasmic localization of TAZ. To confirm that the compartmentalization of TAZ to the cytoplasm is not due to an increase in nuclear size, we measured the nuclear size of hNK cells treated with hiltonol. Interestingly, the nucleus was significantly smaller in hiltonol-treated hNK cells (Figure S3C,D, Supporting Information), thus authenticating the ratio of TAZ distribution between nucleus and cytoplasm. Next, we performed a western blot analysis of TAZ and its direct upstream inactivating kinase, LATS1, and showed increased phosphorylation of both LATS1 and TAZ (Figure 2G). This implies activation of LATS1 (phosphorylation at Serine 909) and inhibition of TAZ (phosphorylation at Serine 89) in NK cells treated with hiltonol. Since MST-1 is the upstream activating kinase of LATS1, we also analyzed and showed a slight increase in MST-1 phosphorylation status (Figure S3E, Supporting Information), hence, supporting an overall activation of Hippo-TAZ pathway in hiltonol-treated NK cells.

Since knockdown of TAZ increases NK cytotoxicity, we reasoned that hiltonol-induced TAZ cytoplasmic compartmentalization should correspond to a reduction in TAZ-mediated nuclear activity resulting in enhancement of NK cytotoxicity. Simultaneously, we showed that hiltonol treatment induced significant nuclear localization of Eomes (Figure S3F, Supporting Information), a transcription factor responsible for reduced PD-1 expression,[3] which resulted in early enhancement of NK cytotoxicity against cancer.[1] Eomes is also one of the key transcription factors regulating expression of perforin and granzyme B.[44] To determine the functional effect of hiltonol on NK cells, we pretreated NK cells with hiltonol and performed a cytotoxicity assay with K562 cells. There was a significant increase in the a) production of granzyme and perforin, b) killing of K562 cells, and c) binding of NK-K562 (Figure 2H–J; Figure S3G, Supporting Information). Interestingly, a high dose of hiltonol (25 μg mL^{-1}) reduced enhancement of NK cytotoxicity against target cells (Figure 2I). This was consistent with reports that high dosage of Poly-I:C/hiltonol tends to reduce the cytotoxicity against target cells.[45–48] Henceforth, we focused on 5 and 10 μg mL^{-1} of hiltonol for experiments on functional analyses (e.g., cancer killing assays). As YAP expression in T cells was shown to only emerge after activation,[33,35,36,39] we next performed an RT-PCR on hNK cells treated with hiltonol and used IL15 as an activation control. Interestingly, YAP was not

as means ± SEM. $n = 4$ for (C), and $n = 5$ for (D). E) Taz knockdown increased granzyme and perforin expression in NK-92 cell. The graph represents means ± SEM and $n = 6$ for all conditions. F) The proliferation (purple) of NK-92 cells, as indicated by Ki67, decreased only with TAZ overexpression. However, the viability (blue) of NK-92 cells were not affected after TAZ knockdown or overexpression. The graph represents means ± SEM and $n = 5$ for all conditions. G) (Left) TAZ knockdown increased NK-92 cell cytotoxicity (higher K562 death). The graph represents means ± SEM and $n = 8$. (Right) Representative flow cytometric graphs show TAZ knockdown increased NK-92 cytotoxicity, respectively. Refer to Figure S2 of the Supporting Information for cytotoxicity assay gating strategy using FVD506 dead cell staining. H) TAZ knockdown increases NK-92 cell cytotoxicity in Calcein-AM release assay. Unpaired Student's *t*-test was used, $n = 4$ I) RT-PCR analysis shows no compensatory YAP expression in TAZ knockdown cells. For all graphs, $*p < 0.05$, $**p < 0.01$, and $****p < 0.0001$.

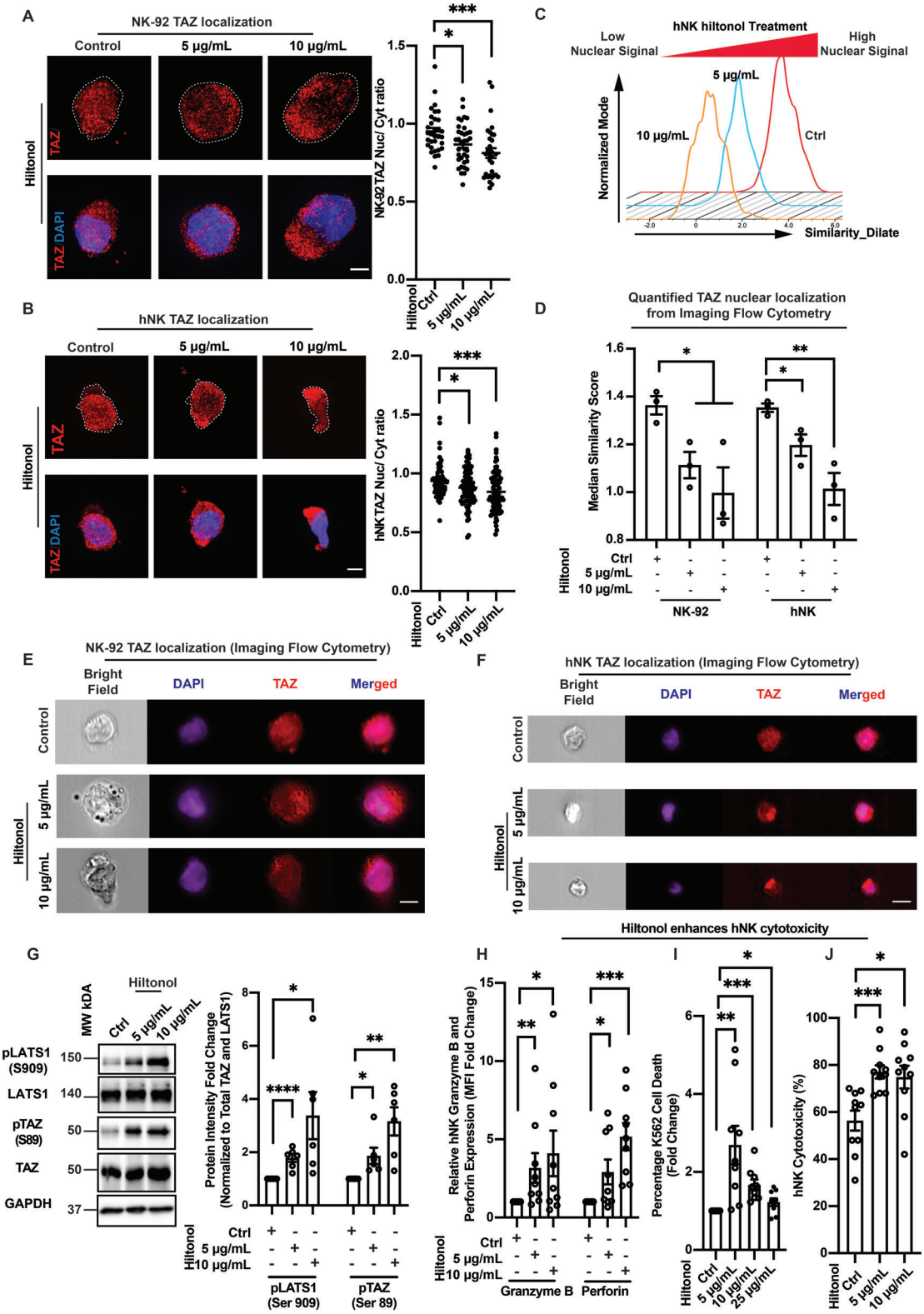

Figure 2. dsRNA mimic, hiltonol, induces cytoplasmic compartmentalization of TAZ and increases NK cytotoxicity. A) Immunofluorescence staining of TAZ in NK-92 cells shows increased cytoplasmic localization of TAZ with hiltonol treatment, Scale bar = 5 μm. The white dotted lines demarcate cell periphery. Quantification on the right represents means ± SEM and n = 32, 36 and 31 for ctrl (control), 5 μg mL^{-1} hiltonol and 10 μg mL^{-1} hiltonol, respectively. B) Immunofluorescence staining of TAZ in hNK cells shows increased cytoplasmic localization of TAZ upon hiltonol treatment. Scale bar = 5 μm. The white dotted lines demarcate cell periphery. Quantification on the right represents means ± SEM and n = 74, 82, and 85 for ctrl, 5 μg mL^{-1}

expressed in any treatment condition (Figure S3H, Supporting Information).

Altogether, we showed that hiltonol treatment resulted in significant induction of cytoplasmic compartmentalization of TAZ, which was associated with enhanced NK cytotoxicity. Next, we aimed to determine mechanistically, how hiltonol induced TAZ cytoplasmic compartmentalization.

2.3. Hiltonol Induces NK Actin-Based Contractility and ROS Production Through ERK1/2

The study of dsRNA mimic in immune cells has thus far mainly focused on its downstream proinflammatory effects.[7,8,49] However, the mechanisms associated with dsRNA signaling, for example on cellular contractility, has hitherto remained ambiguous, although reported.[18,21,22] We have previously demonstrated that the presence of cancer cells enhanced intracellular contractility of NK cells, which promoted nuclear compartmentalization of Eomes.[1] Here, our observation that hiltonol induces Eomes nuclear localization (Figure S3F, Supporting Information) hints that hiltonol treatment activated intracellular contractility for early cytotoxicity response. An enhancement of intracellular contractility was also indicated by the observation that hiltonol-treated NK cells have a smaller nuclear area (Figure S3C,D, Supporting Information) and this is supported by a previous study, which suggested that intracellular contractility compresses the nucleus.[50] TAZ is a transcription cofactor that can also be mechanically regulated;[29,30] thus we hypothesized that hiltonol-treatment simultaneously induces a concerted effect on a biochemical pathway (through LATS1 phosphorylation) and a mechanical pathway (through enhancement of intracellular contractility).

To verify whether and how contractility was enhanced, we treated NK-92 cells with hiltonol and assayed for actin recoil velocity by performing laser ablation on actin filaments (**Figure 3**A). The actin was labeled to ensure specific measurement of actin tension. The recoil velocity directly correlates with intracellular tensional force based on actin-mediated contractility exerted by actin filaments.[1,51] We found that hiltonol dose-dependently induced a significant increase in the NK-92 actin recoil velocity (Figure 3B; Videos S1–S3, Supporting Information). Likewise, hNK cells showed a similar dose-dependent response to hiltonol treatment (Figure 3C; Videos S4–S9, Supporting Information). Since the nonmuscle myosin light 2 (MLC2) chain generates intracellular contractile forces through RhoA activation,[52] we next verified if MLC phosphorylation and RhoA activation were induced by hiltonol treatment. We found that hiltonol significantly increased both the MLC2 phosphorylation (Figure 3D) and the active form of RhoA (RhoA-GTP) (Figure 3E). Since the activity/phosphorylation levels of myosin light chain or RhoA activation can, but not necessarily always result in changes in cell contractility, we directly measured cellular contractility by performing a traction force microscopy (TFM). Indeed, treatment of NK-92 cells with hiltonol showed an increased force generated per area of the cell (Figure S4, Supporting Information).

Next, we determined the mechanism by which hiltonol activates intracellular contractility. It has been reported that systemic activation of mouse TLR3 resulted in ERK1/2 activation and MLC phosphorylation in aortic vascular smooth muscle cells.[22] We perceived this could be conserved in NK cells since the common lymphoid progenitor from which NK cells differentiated are derived from the mesoderm, like muscle cells. Furthermore, hiltonol treatment increased the expression of TLR3 (Figure S3A, Supporting Information).To verify this possibility, we analyzed ERK1/2 phosphorylation after hiltonol treatment, showing a dose-dependent increase in ERK1/2 phosphorylation (Figure 3F) and this was consistent with a previous study.[53] Next, we directly inhibited ERK1/2 phosphorylation with U0126 and measured the actin recoil velocity. We found that inhibition of ERK1/2 drastically reduced hiltonol-induced intracellular contractility (Figure 3C). Furthermore, treatment of NK-92 cells with increasing doses of U0126 significantly reduced RhoA activation, showing reduction in RhoA-GTP (Figure 3G). Hence, ERK1/2 activation is responsible for RhoA-induced intracellular contractility in NK cells.

ROS production has been shown to activate ERK1/2.[54,55] However, recent evidence suggests that ERK1/2 could also reciprocally induce ROS production,[56,57] forming a positive feedback loop. A moderate increase in the level of ROS in NK cells was also proposed to improve NK cell division and function.[58–60] Hence, whether ERK1/2 activation directly correlates with ROS production after hiltonol treatment is of potential interest. We treated hNK cells with hiltonol and/or U0126, and measured the cytoplasmic and mitochondrial ROS production with Dihydroethidium (DHE) staining and MitoSOX staining, respectively. Interestingly, both DHE and MitoSOX staining showed an increase in cytoplasmic ROS production, which was inhibited by U0126 (Figure 3H,I). These observations suggest that hiltonol directly enhances NK cytotoxicity (Figure 2H–J). Nevertheless, the increase in ROS continued to be significant at 25 μg mL^{-1} of hiltonol treatment (Figure 3H,I), although higher dose of hiltonol reduced NK cytotoxicity (Figure 2I). Hence, despite continuous increase in cytotoxic molecules (e.g., perforin and granzyme)

hiltonol and 10 μg mL^{-1} hiltonol, respectively. Data are representative of three hNK donors. C,D) Representative imaging flow cytometric histogram (C) and quantification (D) of E and F, showing TAZ compartmentalization to the cytoplasm of NK-92 (E) and hNK (F) cells with hiltonol treatment. The graph represents means ± SEM, and $n = 3$ for NK-92 cells, and three hNK donors were used for hNK cells. For each n, 3000 to 5000 cells were imaged for quantification. The "similarity dilate" values were calculated according to nuclear translocation wizard in IDEAS 6.0 software. (E,F) Representative images of imaging flow cytometry showing TAZ compartmentalization to the cytoplasm of NK-92 (E) and hNK (D) cells with hiltonol treatment. Scale bar = 10 μm. G) Immunoblot analysis shows increased LATS activation (pLATS1) and increased TAZ inactivation as pTAZ increases in NK-92 cells treated with hiltonol. The graph represents means ± SEM, and $n = 6$. H) Hiltonol treatment increases hNK granzyme B and perforin expression as indicated by expression fold-change of the MFI (mean fluorescence index). The graph represents means ± SEM, and $n = 9$ individual experiments representative of three hNK donors. I) Lower doses of hiltonol treatment (5 and 10 μg mL^{-1}) induce higher hNK cytotoxicity toward model target, K562 lymphoblast cells. The graph represents means ± SEM, and $n = 9$ individual experiments representative of three hNK donors. J) Hiltonol increases hNK cytotoxicity in Calcein-AM release assay. $n = 9$ individual experiments representative of three hNK donors. For all graphs, $*p < 0.05$, $**p < 0.01$. $***p < 0.001$ and $****p < 0.0001$.

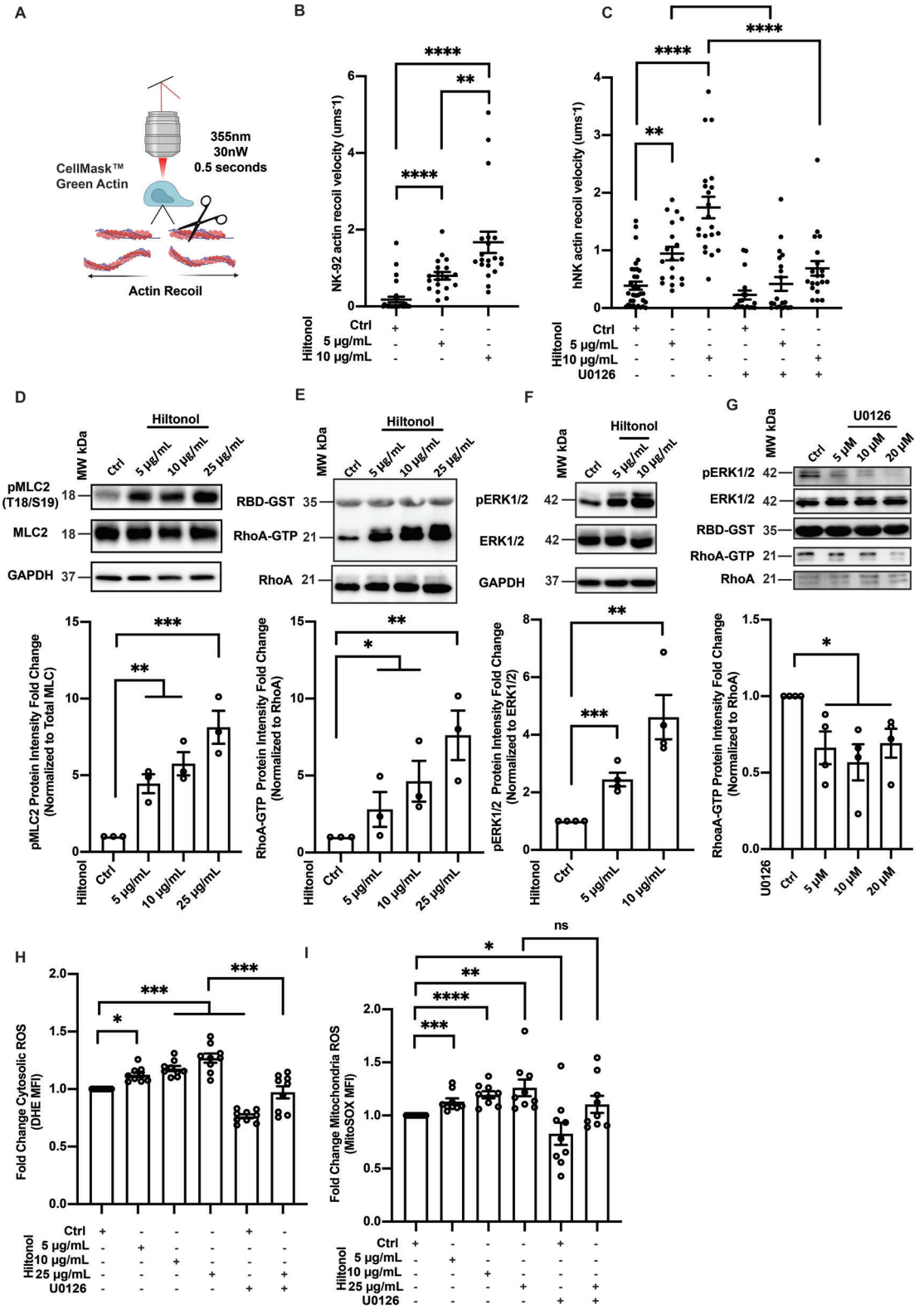

Figure 3. Hiltonol induces NK actin-based contractility and ROS production through ERK1/2. A) Schematic showing laser ablation of NK cells with actin filaments labeled with CellMask green actin. The scissors represent laser ablation site and arrows represent direction of actin recoil. Details can be found in the Experimental Section (Laser Ablation of NK Cell Actin Filaments). B) Hiltonol treatment increases the initial recoil velocity of laser ablated NK-92 actin. The graph represents means ± SEM, and $n = 29$, 19, 20 for ctrl, 5 μg mL^{-1} hiltonol and 10 μg mL^{-1} hiltonol, respectively. C) Hiltonol treatment increases the initial recoil velocity of laser ablated hNK actin. ERK inhibitor U0126 (10 μM) reduced the increase in initial recoil velocity. The graph

due to hiltonol treatment (Figure 2H), high ROS may be self-cytotoxic to NK cells and this limits NK activation/cytotoxicity. Further studies are required to elucidate detailed mechanistic understanding on how high ROS levels limit NK cytotoxicity, and to determine the optimal level of ROS for maximal NK cytotoxicity.

Taken together, we suggest that hiltonol-treated NK cells are associated with higher actin-based intracellular contractility with possible synergy between ERK1/2 activation and moderate ROS production, which corresponded to the increase in NK cell cytotoxicity. Next, it was pertinent to elucidate how enhanced actin-based contractility promoted LATS1 phosphorylation, which in turn affected TAZ subcellular localization.

2.4. Activation of Intracellular Contractility by Hiltonol Probably Reduced LATS1-Actin Association and Sequestered TAZ in the Cytoplasm

It was previously shown that the TAZ homolog, YAP, responds to mechanical forces and compartmentalizes to the nucleus of fibroblast cells.[34] However, we have thus far demonstrated that enhanced contractility (Figure 3A–E) correlated with TAZ cytoplasmic compartmentalization, and promoted LATS1 phosphorylation (Figure 2). Furthermore, another study showed enhanced YAP cytoplasmic localization in response to enhanced contractile force during cardiomyocyte differentiation.[61] We reasoned that intracellular contractility in NK cells probably activated a concerted mechanism linking mechanical contractility to the biochemical regulation of TAZ.

Since ERK1/2 activation was associated with hiltonol-induced RhoA activation and contractility, we first inhibited ERK1/2 with U0126 and analyzed TAZ and LATS1 phosphorylation. As shown in **Figure 4**A, U0126 treatment reduced TAZ and LATS1 phosphorylation in NK-92 cells, suggesting an increase in TAZ nuclear localization. Next, we tested whether direct pharmacological inhibition of myosin-based contractility with blebbistatin would impact the subcellular localization of TAZ in hNK cells. Indeed, we observed a significant nuclear recompartmentalization of TAZ when myosin-contractility was inhibited by blebbistatin (Figure 4B). This is in contrast to hiltonol induced TAZ cytoplasmic compartmentalization as demonstrated in Figure 2. Furthermore, western blot analyses showed that hiltonol-induced LATS1 phosphorylation was also slightly downregulated by blebbistatin (Figure 4C). These observations suggest an association between cell force (intracellular contractility) and promotion of TAZ sequestration in the cytoplasm, which is in line with a previous study showing blebbistatin-induced nuclear localization of YAP/TAZ in MDCK cells.[62] We further verified the role of ECM-induced intracellular contractility by plating NK-92 cells on hard and soft, fibronectin-coated poly(dimethylsiloxane) (PDMS) surface, and observed TAZ localization by confocal imaging and western blot analyses. Fibronectin has been shown to promote NK cell spreading[63] and migration[64] by engaging NK cell integrins, and it is known that integrin engagement activates actin-based intracellular contractility. As envisaged, we found that NK-92 cells plated on soft surfaces showed higher TAZ nuclear localization with lesser TAZ phosphorylation (Figure 4D,E).

LATS1 kinase is an actin-binding protein, which antagonizes actin polymerization,[65] suggesting that LATS1 activation through phosphorylation requires either i) actin depolymerization or ii) its dissociation from F-actin filaments. Since LATS1 is a direct inactivation kinase of TAZ but was activated with hiltonol treatment (Figure 2G), it is conceivable that enhanced contractility would reduce the association of LATS1 to actin and the "freed" LATS1 becomes phosphorylated (Figure 4F). Furthermore, studies on GPCRs identified the integrity of the actin cytoskeleton as a repressor of the Hippo pathway.[66] In addition, although there was a slight increase in MST1/2 activation (Figure S3E, Supporting Information), the increased LATS1 activation was much more robust (Figure 2G). To corroborate these observations, we performed a flow cytometric proximity ligation assay (PLA). PLA combined with flow cytometry allows quantitative analysis of proteins in proximity, as close as 40 nm.[67] We found that treating NK cells with hiltonol significantly reduced the association of LATS1 and actin (Figure 4G), implying that enhanced intracellular contractility releases LATS1 from F-actin.

Thus far, we have shown that NK cells express TAZ, and hiltonol treatment sequesters TAZ to the cytoplasm. Activation of contractility through ERK1/2 probably resulted in reduced LATS1-actin association, which correlated with higher LATS1 phosphorylation and concomitant TAZ phosphorylation. We next sought to determine how TAZ limits NK cell cytotoxicity.

2.5. TAZ-Induced c-Myc Activity Regulates NK Cell Inhibitory Receptor, KIR3DL1

One of the mechanisms by which NK cytotoxicity is regulated involves the balance of activating (e.g., NKG2D, DNAM-1) and inhibitory (e.g., NKG2A, TIGIT, PD-1, KIR2DL1, and KIR3DL1) surface receptors.[2,10] We hypothesized that hiltonol-induced TAZ cytoplasmic sequestration could regulate the expression of one or multiple surface receptors on NK cells. To test this, we analyzed the expression of various major surface receptors. Interestingly, while no upregulation of NK activating receptors was observed (**Figure 5**A), we noticed significant downregulation of the inhibitory receptors like KIR3DL1 (Figure 5B). PD-1 has been reported to be expressed on primary human NK cells,[68] making it an invaluable target for immunotherapy. Although we observed low PD-1 surface expression in most donor hNK cells, there was still a significant decrease in PD-1 surface expression in hiltonol-treated hNK cells (Figure 5B). In addition, the downregulation of

represents means ± SEM, and $n = 34$, 19, 21, 18, 20, 20 for each column of the graph, respectively. D–F) Immunoblots show that hiltonol treatment increases NK-92 pMLC2 (phosphorylated myosin-like chain 2) that is correlated with RhoA activation (RhoA-GTP) and ERK activation (pERK1/2). The graph below each immunoblot represents means ± SEM, and $n \geq 3$. G) Immunoblot showing that U0126 treatment reduces pERK1/2 levels, which is correlated to reduced RhoA activation (RhoA-GTP). The graph below represents means ± SEM, and $n = 4$. H,I) Hiltonol treatment increases hNK cytosolic ROS as indicated by DHE staining (H) and mitochondria ROS as indicated by MitoSOX staining (I). This was inhibited with the ERK inhibitor U0125. The graph represents means ± SEM, and $n = 9$ representative of three hNK donors. For all graphs, $^{*}p < 0.05$, $^{**}p < 0.01$. $^{***}p < 0.001$ and $^{****}p < 0.0001$.

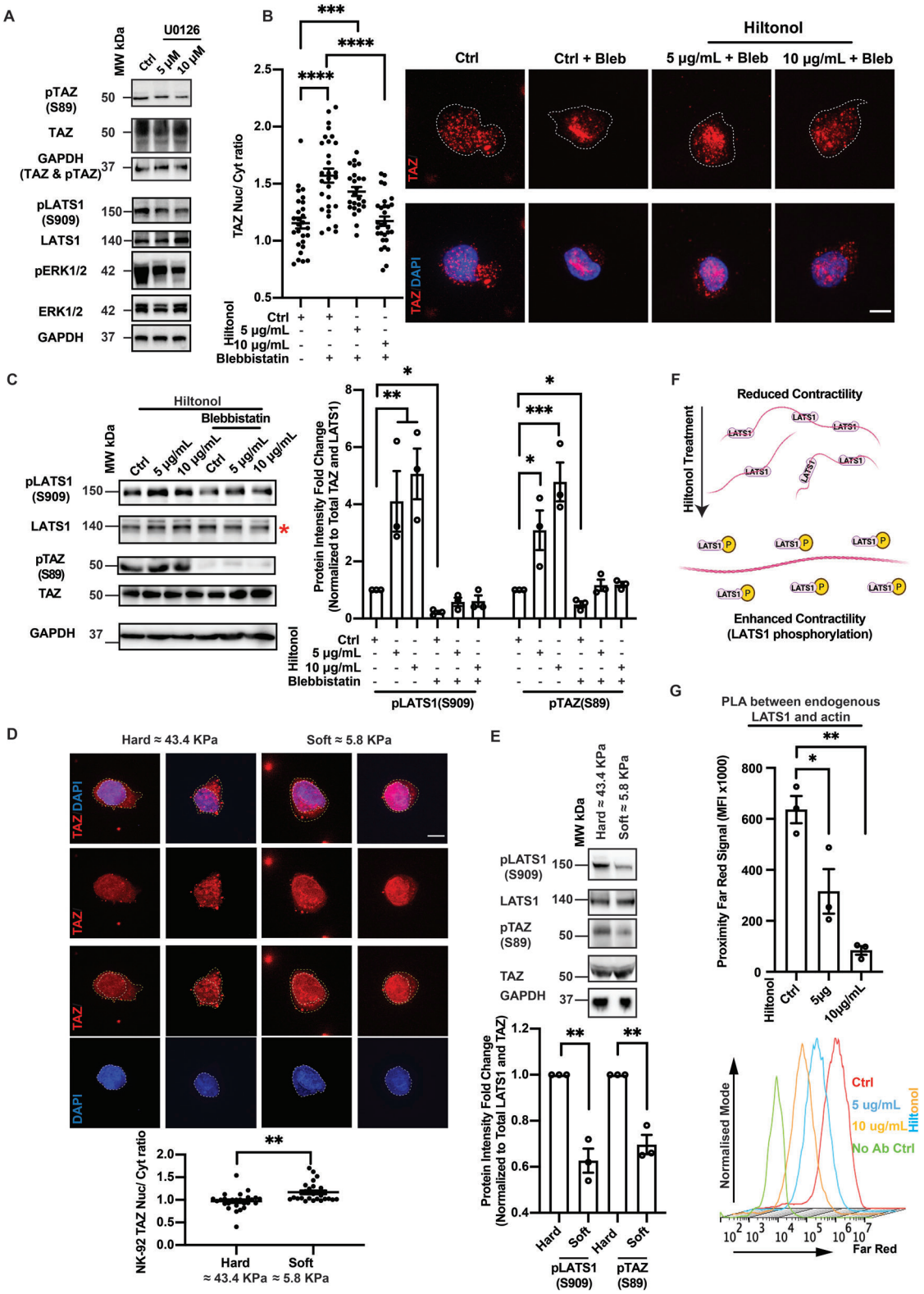

Figure 4. Activation of intracellular contractility by hiltonol probably reduced LATS1-actin association and sequesters TAZ in cytoplasm. A) Immunoblot showing U0126 treatment (10 μM) overnight reduces TAZ phosphorylation and LATS1 phosphorylation in NK-92 cells, $n = 3$. B) Quantification (left) and representative images (right) show that myosin inhibitor, blebbistatin (40 μM) treatment overnight, increases TAZ nuclear localization in NK-92 cells. The white dotted lines outline the cell periphery. Scale bar = 5 μm. The graph represents means ± SEM, and $n = 27, 29, 24, 29$ for each column. C) Immunoblot shows that increases in pLATS1 and pTAZ with hiltonol treatment were blocked by the addition of blebbistatin (40 μM). The red asterisk indicates the

PD-1 was consistent with transcription factor, Eomes-mediated suppression of PD-1,[3] and here we have also shown that Eomes localizes to the nucleus of hiltonol-treated NK cells (Figure S3F, Supporting Information), which was associated with the suppression of PD-1. In addition, to reconcile these observations with the functional outcome of NK, we analyzed CD56 (NK maturation marker) and CD16 (NK antibody-dependent cell-mediated cytotoxicity marker) expressions on NK cells and showed that hiltonol treatment did not alter their expressions (Figure S5, Supporting Information). On the other hand, the downregulation of KIR3DL1 raised the possibility that as a transcription cofactor, TAZ, might have induced downstream genes that regulated the expression of KIR3DL1. We further confirmed this by knocking down TAZ in NK-92, which significantly reduced the surface expression of KIR3DL1 (Figure 5C). To strengthen our claim, we inhibited TAZ activity with the YAP/TAZ inhibitor, verteporfin. Verteporfin is a suppressor of the YAP/TAZ-TEAD complex and activator of 14-3-3 that sequesters TAZ in the cytoplasm.[69–72] Treatment of NK cells with verteporfin enhanced NK cell cytotoxicity against K562 cells (Figure 5D) and upregulated the production of granzyme and perforin (Figure 5E). Additionally, verteporfin reduced KIR3DL1 surface expression (Figure 5F, red box), whereas PD-1 expression was unaffected. These observations suggest that one of the possible ways TAZ limits NK cell cytotoxicity is through the sustenance of inhibitory receptor, KIR3DL1.

c-Myc is a downstream transcription factor under TAZ control.[37,73,74] For example, nuclear accumulation of TAZ upregulated c-MYC expression[73] and TAZ activation resulted in c-MYC-driven hepatocarcinogenesis.[37] Furthermore, a previous study showed that c-Myc binding at the distal KIR promoter during NK-cell development specifically promotes KIR transcription.[75] Hence, we next verified if c-Myc could have an influence on KIR3DL1. To this end, we first tested whether c-Myc inhibition would enhance NK cytotoxicity. We found that inhibition of c-Myc with G3798, increased NK cytotoxicity against K562 cells in a dose-dependent manner (Figure 5G). However, at a high dosage (20 μM), G3798 reduced the cytotoxicity of NK cells (data not shown). Furthermore, low doses of G3798 also resulted in an increase in granzyme B and perforin levels (Figure 5H). In addition, c-Myc inhibition reduced KIR3DL1 surface expression (Figure 5I, red box), without affecting PD-1. Finally, treatment of NK cells with hiltonol was found to directly reduce mRNA transcript levels of c-Myc (Figure 5J,K), suggesting that hiltonol-induced TAZ cytoplasmic compartmentalization resulted in and correlated with reduced c-Myc activity.

Overall, we have shown that TAZ in NK cells positively regulates c-Myc expression and function, which is associated with hiltonol-induced intracellular contractility (Figure 5L). The expression of c-Myc probably sustains the expression of the inhibitory surface receptor, KIR3DL1. Interestingly, the KIR2DL1 inhibitory receptor was not affected (Figure 5B), possibly due to its very low expression on hNK cells (see FMO gatings in the Supporting Information figure). Hence, the regulation of KIR3DL1 surface expression by hiltonol could serve as a possible mechanism to regulate hiltonol-induced NK cell cytotoxicity.

2.6. Hiltonol Induction and c-Myc Inhibition Enhance the Cytotoxicity of NK Cells against Breast and Lung Cancer Cells

As a more stable form of dsRNA, hiltonol has been widely used as a vaccine adjuvant.[19,76] Few studies have demonstrated direct cancer-killing capabilities of hiltonol on cancer cells.[46,47] However, whether hiltonol can participate in NK cell immunomodulation is unexplored. We have shown that hiltonol enhanced NK cytotoxicity, killing the model cell line, K562 lymphoblast (Figure 2I,J). Since we have previously demonstrated a graded NK cell response toward the less and more metastatic lung and breast cancer cells,[1] here we set out to determine if in coculture settings, hiltonol would enhance the cytotoxicity of NK cells toward the more resistant cancer types (lung and breast cancer) and subtypes (metastatic vs nonmetastatic). Furthermore, metastatic lung and breast cancer patient and cells present high HLA ligand expression, and NK cells express high level of KIR3DL1.[77,78] This will provide a direct translational immunotherapeutic advancement.

We pretreated hNK cells overnight (18 h) with hiltonol and then cocultured hNK cells with CFSE-stained lung (H1299 and H1975) and breast (MCF7 and MDA-MB-231) cancer cells (**Figure 6**A). Since Figures 1H and 2J showed consistent results between traditional Calcein-AM release assay and FVD506 staining of dead cells, we utilized FVD506 staining in subsequent cytotoxicity assays. An overnight treatment with hiltonol was based on our previous observation that such a duration of treatment was sufficient to induce a robust early cytotoxic response in NK cells, which correlated with transcription factor (Eomes) nuclear translocation. Furthermore, the less metastatic H1975 lung cancer and MCF7 breast cancer cell lines were easily killed by hNK cells.[1] We found that pretreatment with hiltonol enhanced the cytotoxicity of hNK cells against both the breast and lung cancer cells (Figure 6B i,ii) by about 1.5- to 2.0-fold. Interestingly, this increase remained pronounced even when hNK cells were challenged with the metastatic cancer subtypes (MDA-MB-231 and H1299), which we have previously demonstrated to induce higher and prolonged contractility in NK cells. Consistently, the levels of granzyme B and perforin were increased (Figure 6B iii,iv). Nevertheless, the highly metastatic MDA-MB-231 could not induce an increase in hNK perforin (Figure 6B iv) despite hNK cells displaying higher killing capacity with hiltonol treat-

LATS1 protein band. The graph represents means ± SEM and $n = 3$. D) NK-92 cells seeded on fibronectin-coated hard substrates show lower nuclear localization compared to that of soft substrate. The graph represents means ± SEM, $n = 25$ and 26 for hard and soft substrates, respectively. Unpaired Student's *t*-test was used to compare between hard and soft substrates. E) Immunoblot shows lesser pLATS1 (S909) and pTAZ(S89) in NK-92 lysates harvested from the soft substrate. The graph at the bottom represents quantification with means ± SEM and $n = 3$. F) Schematic showing enhanced contractility (e.g., with hiltonol treatment) dissociates LATS1 from actin and correlates with increased LATS1 phosphorylation. G) Hiltonol treatment of NK-92 reduces PLA (proximity ligation assay) far red MFI signals, indicating reduced colocalization of LATS1 and actin. The graph represents means ± SEM and $n = 3$. The representative flow cytometry histogram below shows left shift (lesser signal) of peaks with hiltonol treatment. For all graphs, $*p < 0.05$, $**p < 0.01$. $***p < 0.001$ and $****p < 0.0001$.

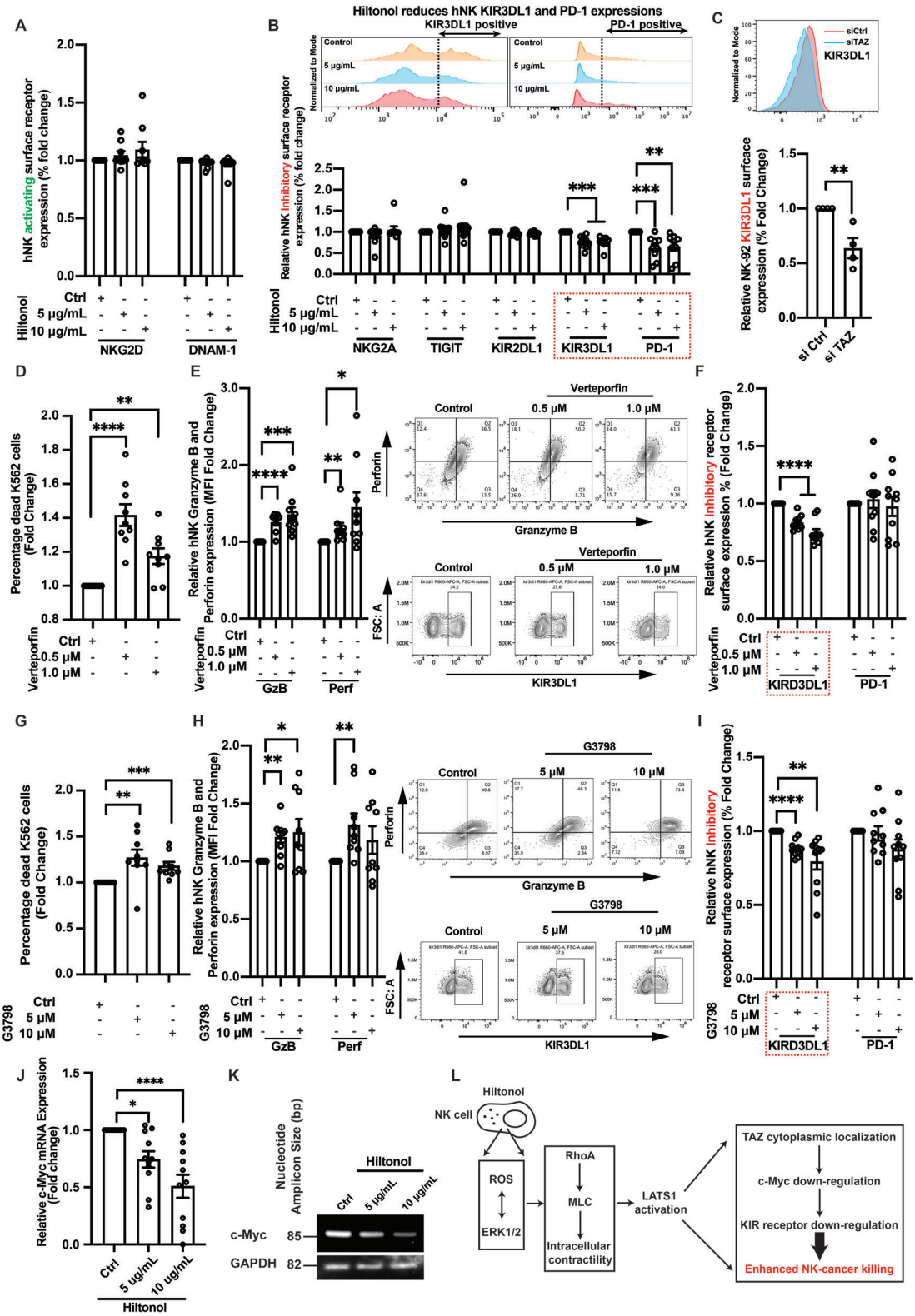

Figure 5. TAZ-induced c-Myc activity regulates NK cell inhibitory receptor, KIR3DL1. A,B) Hiltonol treatment overnight (18 h) did not alter surface expressions of hNK activating receptors, NKG2D and DNAM-1 (A), whereas the inhibitory receptors KIR3DL1 and PD-1 (expressed at low level) were significantly reduced with hiltonol treatment (B), red box. The graph represents means ± SEM and $n = 9$ representative of three hNK donors. The representative flow cytometric histograms for KIR3DL1 and PD-1 for one donor are represented above the graph and the dotted vertical line facilitates the viewing of histogram shifts. C) TAZ knockdown (48 h) in NK-92 cells significantly reduces the inhibitory receptor KIR3DL1 surface expression, whereas PD-

ment (Figure 6B ii). Hence, other mechanisms may be involved in upregulating hNK-cancer cell killing.

Over the years, c-Myc inhibition has become the most appealing anticancer approach in cancer clinical trials. The expression of c-Myc is tightly controlled in normal cells, but becomes dysregulated and overexpressed in most human cancers, making it one of the most important human oncogenes.[79] However, in vivo observations often fall short of in vitro expectation.[79] Since c-Myc is one of the limiting factors in NK cytotoxicity (Figure 5), we cocultured hNK cells and cancer cells in the presence of c-Myc inhibitor (G3798), anticipating c-Myc inhibition to also increase NK cytotoxicity against the cancer subtypes.

Since c-Myc inhibition could induce inherent changes in hNK and cancer cell phenotype, we analyzed the phenotype of hNK cells after G3798 treatment and showed that CD56 and CD16 surface expressions were not significantly affected (Figure S5, Supporting Information). Next, we verified if c-Myc inhibition will result in direct cancer cell death. Interestingly, c-Myc inhibition with G3798 did not cause cancer cell death unless it was applied at a high dose of 20 μM (Figure S6A, Supporting Information) and the highly metastatic H1299 lung cancer cell line was most resistant to c-Myc inhibition. Conversely, c-Myc inhibition did not result in substantial cell death in NK cells, even at a high dose of 20 μM G3798 (Figure S6B, Supporting Information), indicating the robustness of NKs. Since cancer cells were only susceptible to c-Myc inhibitor at a high dose (Figure S6A, Supporting Information) and may present general toxicity for translational studies, we next cocultured hNK cells and cancer cells with G3798 at lower doses (5 and 10 μM) to investigate the specific impact of c-Myc inhibition of hNK on its anticancer activity. We found that c-Myc inhibition induced a dose-responsive increase in hNK-mediated cancer-killing capacity (Figure 6C i,ii). Strikingly, even the metastatic cancer subtypes (H1299 and MDA-MB-231) appear to be susceptible to G3798-induced hNK killing. In addition, the increase in cancer killing capacity also correlated with a moderately increased granzyme and perforin levels (Figure 6C iii,iv). Therefore, our results agree with a previous study that c-Myc blockade with inhibitors suppresses cancer growth and this is further enhanced with combinatorial treatment with anti-PD-1 antibody.[80] Nevertheless, our observation that G3798 treatment induced only a modest increase in granzyme B and perforin production again implicates additional mechanism of hNK-induced cancer killing that remains to be explored.

Finally, to test whether hiltonol pretreatment and c-Myc inhibition can elicit a synergistic effect on cancer-killing, we pretreated hNK cells overnight with hiltonol before coculturing with highly metastatic cancer subtypes (MDA-MB-231 and H1299) in the presence of G3798. Interestingly, an apparent synergistic effect was observed when hNK cells were challenged with MDA-MB-231 cells (Figure S6C, Supporting Information). This effect was less evident with the more resistant H1299 lung cancer cells. Since c-Myc is identified as a downstream target influenced by hiltonol treatment, our findings showed amplification (synergy) of the benefits of c-Myc inhibition with hiltonol-mediated antitumorigenic mechanisms.[17,47,81–83]

In conclusion, we have shown that the innate immune NK cells express TAZ but not YAP. The activation of actin-based contractility by the dsRNA mimic immune adjuvant, hiltonol, through ERK1/2 activation and ROS production, possibly led to TAZ cytoplasmic compartmentalization and enhanced NK cytotoxicity in vitro. This was consistently observed with reduced LATS1-actin association and increased LATS1 activation and TAZ inactivation. In the absence of hiltonol, homeostatic control of actin-based contractile forces maintains c-Myc activity, resulting in the surface expression of the inhibitory receptor KIR3DL1. Our findings provide an avenue for therapeutic translational advances as our results indicate that sensitizing hNK cells to hiltonol could subdue both metastatic and non-metastatic cancer types (breast and lung) and the corresponding subtypes. **Figure 7** provides a model to summarize our findings.

3. Discussion

The roles of cell "force" in regulating pathophysiological processes are gaining interest and warrant urgent attention. Various NK cell-related immune diseases result from aberrant regulation of proteins that control cytoskeletal force.[28] Here we provide empirical evidence supporting NK cell intracellular contractility modulated with an immune adjuvant, hiltonol. The direct consequence of this is the cytoplasmic sequestration with phosphorylation and inactivation of TAZ protein, and subsequent reduction in expression of the surface inhibitory receptor, KIR3DL1. Interestingly, we also observed an indirect downregulation of an important inhibitory receptor, PD-1, that was associated with an increase in Eomes nuclear localization. Surmise to say, pretreatment of NK cells with hiltonol can upregulate the cytotoxicity of NK cells to target and kill lymphoblast and breast and lung cancer cells.

The mechanistic role of "force" in triggering YAP/TAZ localization in cell systems is gaining attention since various studies

1 surface expression is not affected. The graph represents means ± SEM and $n = 4$. D–F) Overnight (18 h) treatment with YAP/TAZ inhibitor, verteporfin, increases hNK cytotoxicity against K562 lymphoblasts (D), with concomitant increase in expressions of granzyme B and perforin (E). On the other hand, only KIR3DL1 (red box) decreased with verteporfin treatment (F). The graph represents means ± SEM and $n = 9$ representative of three hNK donors. The flow cytometric layouts represent the increased granzyme B and perforin expression in hNK cell treated with verteporfin and reduced KIR3DL1 expression in hNK cells. G–I) The c-Myc inhibitor, G3798, treatment overnight (18 h) increases hNK cytotoxicity against K562 lymphoblast (G), with corresponding increase in the expressions of granzyme B and perforin (H). On the other hand, only KIR3DL1 (red box) decreases with G3798 treatment (I). The graph represents means ± SEM and $n = 9$ representative of three hNK donors. The flow cytometric layouts represent the increased granzyme B and perforin expression in hNK cell treated with G3798 and reduced KIR3DL1 expression in hNK cells treated with G3798. J,K) Hiltonol treatment reduces c-Myc mRNA expression. The graph represents means ± SEM and $n = 11$ representative of four hNK donors. A representative gel blot (out of $n = 4$) was shown and the size markers represent the nucleotide amplicon size and not gene size. L) Schematic showing the mechanistic enhancement of NK cell cancer killing through ROS-, ERK1/2-induced RhoA-MLC enhancement of intracellular contractility. Enhanced intracellular contractility activates LATS1 to inactivate TAZ through cytoplasmic localization that resulted in downregulation of the inhibitory KIR receptor. For all graphs, $*p < 0.05$, $**p < 0.01$. $***p < 0.001$ and $****p < 0.0001$.

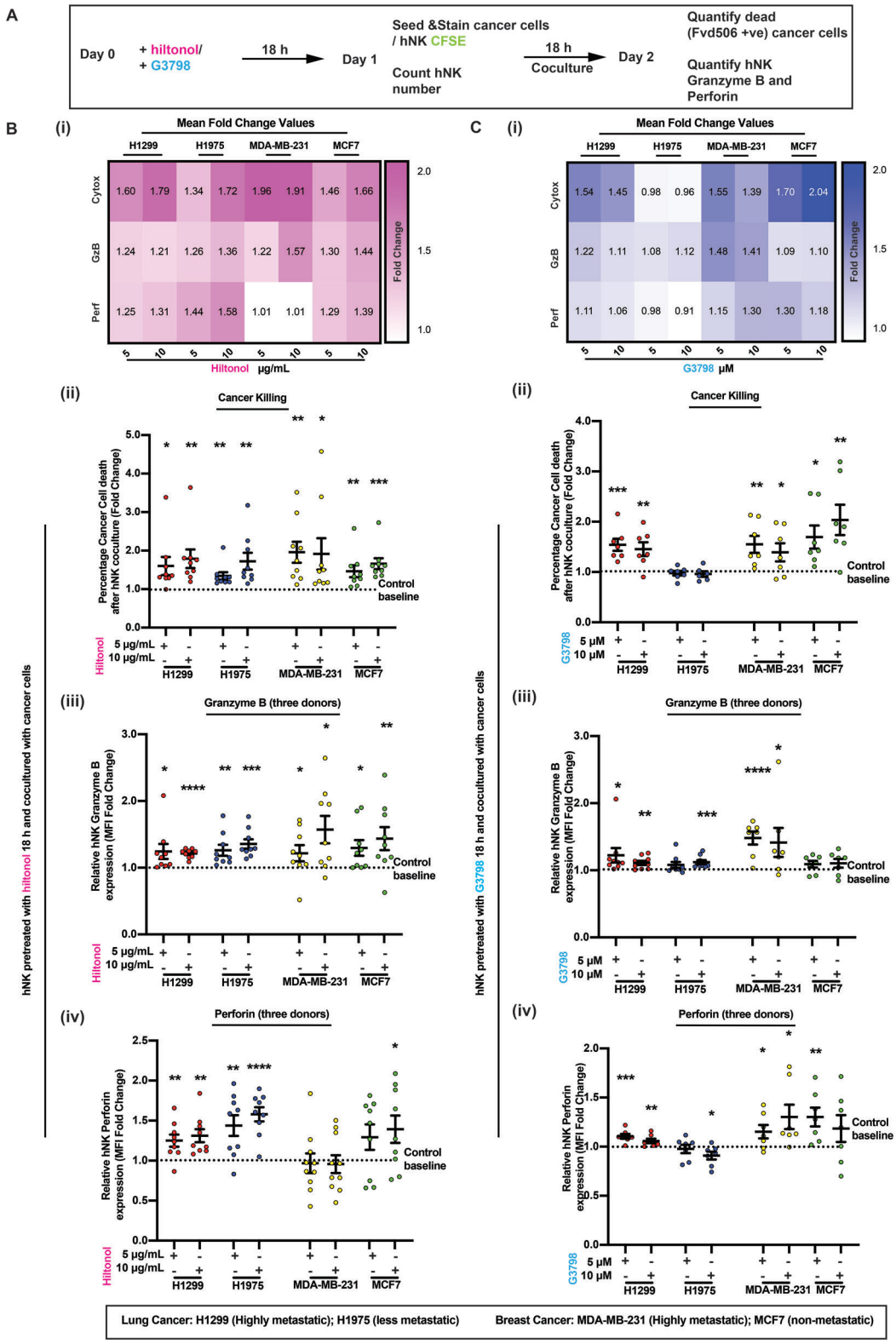

Figure 6. Hiltonol treatment and c-Myc inhibition enhance cytotoxicity of NK cells against metastatic and less metastatic breast and lung cancer cells. A) Schematic flow showing the pretreatment of hNK cells with hiltonol or G3798 overnight (18 h) before coculturing with cancer cells (seeded for at least 8 h) to analyze cancer cell death or hNK granzyme B and perforin production. The cell type to be analyzed was labeled with CFSE to allow easy differentiation during flow cytometric analysis and the FVD506 dye was used to stain dead cells. Refer to Figure S2 of the Supporting Information for gating strategy to identify CFSE staining dead cancer cells. B) Hiltonol pretreatment increases hNK cytotoxicity toward all lung (H1299 and H1975) and breast (MCF7

have shown that force does not seem to act alone in this process. It was previously demonstrated that force applied on the nucleus was sufficient to trigger YAP nuclear localization.[34] We have previously shown that the transcription factor, Eomes, entered the NK nucleus as a consequence of increased intracellular contractility.[1] Although YAP/TAZ can be regulated canonically by a series of kinases (MST1/2 and LATS1/2),[30] how these kinases are regulated by cell force is unclear. YAP has been shown to suppress T-cell activation and differentiation,[35,36,84] but we have shown that NK cells express TAZ, but not YAP. With the enhancement of RhoA-MLC2 induced intracellular contractile force, TAZ was found to be sequestered in the cytoplasm instead of entering the nucleus. Our findings agree with other studies whereby force alone may not lead to YAP nuclear localization. In a study with gastric cancer cells, the presence of cadherin 1 was purportedly required for YAP nuclear localization as a result of gain-of-function with RhoA activation.[85] In yet another cardiomyoblast differentiation model, intracellular contractile force was shown to sequester YAP in the cytoplasm to switch the cellular process from growth to differentiation.[74] In addition, the timescale of activation of cells by force may also affect YAP/TAZ intracellular localization. Whereas, in one study, force was applied for 5 min by atomic force microscopy and YAP was found to localize into the nucleus of fibroblast cells.[34] In our study, hiltonol-induced activation of contractility was investigated over a time scale of 18 h. Hence, this may allow for the activation of "place" and "pace-makers" such as kinase activation cascade to regulate TAZ localization. Here, we show that "force" promotes the cytoplasmic sequestration of TAZ in NK cells. Importantly, our results provided mechanistic explanations on how force activates the inactivating kinase, LATS1, to inactivate TAZ. Since LATS1 is known to bind to actin,[65] the conceptual understanding is that we view actin as a relaxed string with LATS1 bound to it. We perceive that activation of force through RhoA-induced MLC2 activation creates "tension" on the actin "string" that results in the "release" of LATS1 from actin (see Figure 4F) and this event correlated with LATS1 activation through phosphorylation (see Figure 4C). At this juncture, we do not yet have an explanation on how the dissociation of LATS1 from actin results in its activation. However, it is conceivable that the binding of LATS1 to actin directly resulted in a "microenvironment" that created intense competition for the abundance of ATP available for activation of actin and LATS1. Actin is well known to bind ATP or ADP monomers tightly.[86] Two studies with small inhibitors of LATS1 also demonstrated that competition for ATP inhibits LATS1 activation.[87,88] Hence, it is likely that the "microenvironment" consisting of actin and LATS1 favors actin activation. The dissociation of LATS1 from actin may expose LATS1 ATP-binding sites and facilitate its activation through phosphorylation (Figure 4D). On the other hand, the activation of LATS1 following its dissociation from actin may depend on other scaffold proteins that also bind to actin (e.g., angiomotins). It is known that the scaffold protein angiomotin and LATS1 are able to activate each other.[89,90] Importantly, the mutant defective in angiomotin which was unable to bind F-actin, was shown to inactivate YAP in various cell models and the deletion of LATS1 had an additive effect.[91] Hence, it is possible that other components of Hippo-TAZ signaling pathway may be regulated by enhancement of intracellular contractility through dissociation from actin. Nevertheless, whether and how LATS1 and actin compete for ATP, and whether the LATS1 activation through enhanced contractility requires other kinases that bind to actin, warrants further investigation. Furthermore, whether the dynamics of LATS1 recruitment to actin is affected by contractility could also be studied in detail in future by using various high resolution and quantitative microscopy techniques (e.g., fluorescence recovery after photobleaching).

An interesting question that remains to be answered in this study is whether TAZ knockdown would increase the sensitivity of NK cells to cytokines. This is important because cytokine receptor signaling gene sets were enriched in a Yap-cKO tumor infiltrating T cell, which suggested that responsiveness to cytokine receptor engagement were enhanced.[35] As NK cells are now recognized to elicit anticancer capabilities, whether and how different combination of cytokine cocktails can enhance or dampen NK cells in the presence and absence of TAZ, remains unexplored.

TLR3, MDA-5, and RIG-1 are well-studied PRRs that activate antiviral responses in NK cells.[17] However, what is unclear is how these sensors in particular, TLR3 may activate contractile forces in a context dependent manner. For instance, TLR3 activation by Poly-I:C was reported to activate contractility in aortic smooth muscle cells.[22] Partly inspired by this, we investigated the possibility that NK cells, which lack the force-transducing focal adhesion complex, can still activate contractility through TLR3 activation. Interestingly, we showed that hiltonol was able to increase the contractile force of NK cells, and this was through

and MDA-MB-231) cancer cell subtypes (i) Heatmap showing the increase (fold change) in hNK cytotoxicity (Cytox), granzyme B (GzB), and perforin (Perf) against all cancer cell lines (lung cancer: H1299 and H1975; breast cancer: MDA-MB-231 and MCF7) with hiltonol pretreatment (5 and 10 μg mL^{-1}). The values in each of the heatmap cells are the mean values of data for (ii)–(iv). (ii) Hiltonol treatment increases hNK cytotoxicity against all four cancer cell lines. The dotted horizontal line represents control baseline killing of hNK cells against the four cancer cell lines and is normalized to 1.0. Comparisons are made between each column to the control baseline. The graph represents means ± SEM and $n \geq 9$, representative of three hNK donors. (iii,iv) Hiltonol pretreatment increases hNK granzyme B (iii) and perforin (iv) production in a dose-dependent manner, by ≈50%. Lung cancer cells (H1299 and H1975) induced higher hNK perforin production, while breast cancer cells (MCF7 and MDA-MB-231) induced higher hNK granzyme B levels. The dotted horizontal line represents control baseline killing of hNK cells against the four cancer cell lines and is normalized to 1.0. Comparisons are made between each column to the control baseline. The graphs represent means ± SEM and $n \geq 9$, representative of three hNK donors. C) The c-Myc inhibitor, G3798, enhanced or sustained hNK-induced cancer cell death in all cancer subtypes. (i) Heatmap showing the increase (fold change) in hNK cytotoxicity (Cytox), granzyme B (GzB), and perforin (Perf) against all for cancer cell lines (lung cancer: H1299 and H1975; breast cancer: MDA-MB-231 and MCF7) with G3798 pretreatment (5 and 10 μM). The values in each of the heatmap cells are the mean values of data for (ii)–(iv). Hiltonol was able to enhance more cytotoxicity against breast cancer cells (MCF7 and MDA-MB-231) and induced higher granzyme B and perforin levels in hNK cells (iii, iv). The dotted horizontal line represents control baseline killing of hNK cells against the four cancer cell lines and is normalized to 1.0. Comparisons are made between each column to the control baseline. The graphs represent means ± SEM and $n \geq 6$ representative of three hNK donors. For all graphs, $^{*}p < 0.05$, $^{**}p < 0.01$. $^{***}p < 0.001$ and $^{****}p < 0.0001$.

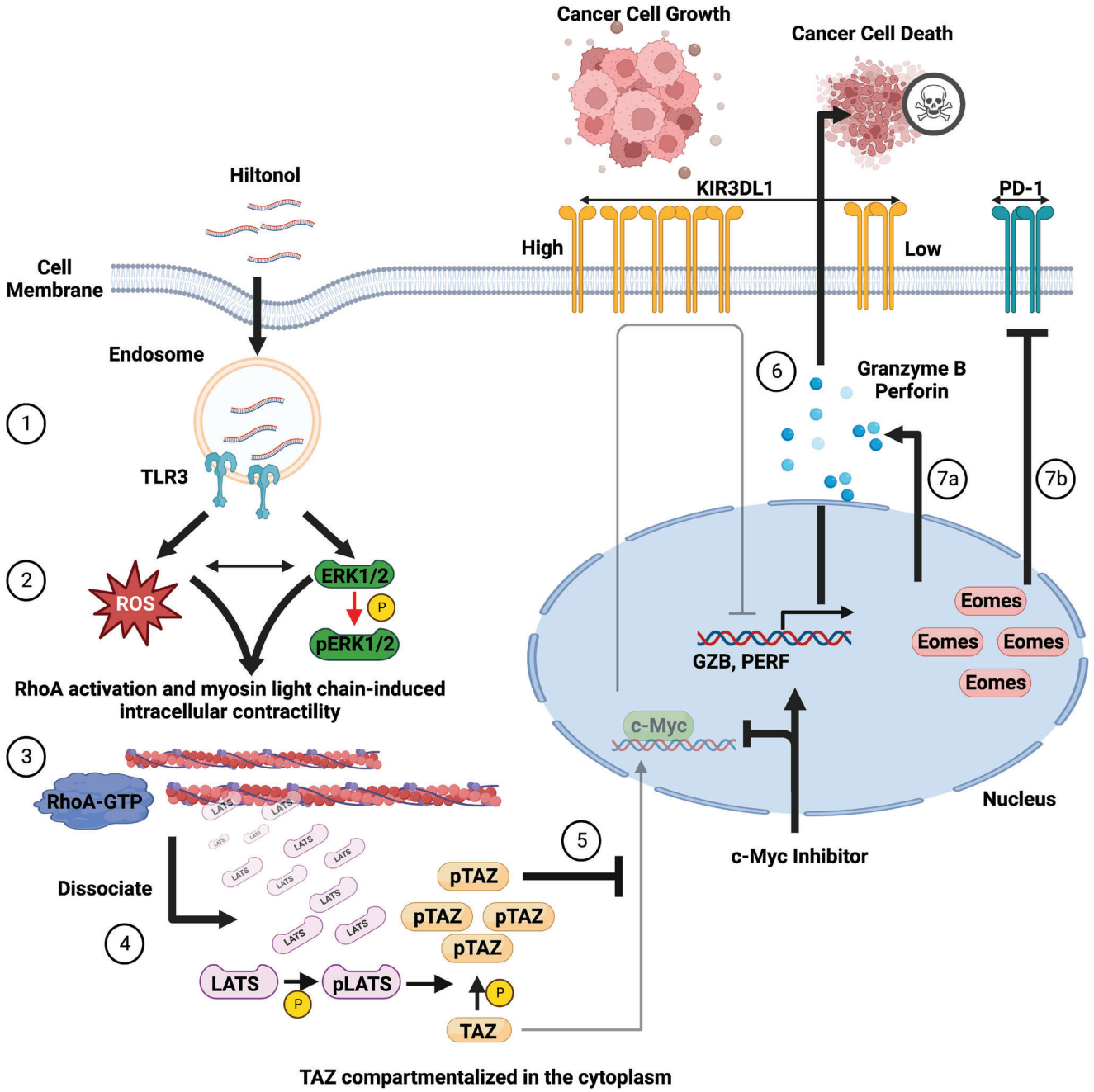

Figure 7. Schematic showing hiltonol treatment enhanced NK anticancer capacity. (1) Hiltonol increases NK cell TLR3 expression that correlated with enhanced ROS (mitochondrial and cytoplasmic) and ERK activation. (2) ROS and ERK activation possibily form a positive feedback loop. (3) ERK activation resulted in RhoA activation and enhanced myosin light chain-based intracellular contractility, probably resulting in (4) the dissociation/reduced recruitment of LATS1 from/to actin. This correlated with LATS1 activation through phosphorylation, which inactivates TAZ through phosphorylation. (5 and 6) Phosphorylated TAZ is unable to enter the nucleus and induce c-Myc activity associated with increased KIR3DL1 expression. This was supported by c-Myc inhibition (with G3798), which resulted in increased expression of GZB (granzyme B) and PERF (perforin). (7a and b) Enhanced contractility also resulted in Eomes nuclear localization and this was associated with reduced PD-1 expression and increased granzyme B and perforin production. Altogether, NK cells treated with hiltonol and c-Myc inhibitor display enhanced cytotoxicity against breast and lung cancer cells.

the activation of RhoA and MLC2. In various cellular and cancer models, TLR3 was also shown to activate small GTPases like RhoA, Cdc42, and Rac1.[92–94] Importantly, what are the functional consequences of enhanced contractility? Although we have shown that TAZ cytosolic localization and Eomes nuclear localization govern the increase in NK cytotoxicity, we do not discount the possibility that various pathways can be activated by contractile forces or through RhoA that is independent of force. For instance, it has been demonstrated that RhoA is required for NF-κB activation[92] and NF-κB itself is regulated by TLR3 activation and

has been shown to promote NK anticancer activities. Interestingly, NK cell activation also depends on other immune subtypes in vivo. For instance, Poly-I:C was shown to activate dendritic cells that subsequently activate NK cells;[81] and the activation of NF-κB was shown to facilitate NK activation by dendritic cells.[95] Importantly, apart from TLR3, other intracellular dsRNA sensors, MDA-5 and RIG-1, are also reported to respond to Poly-I:C (studied using mouse dendritic cell activation)[82] and this purportedly cross-activates NK cells. Hence, it is possible that hiltonol could simultaneously activate the cytosolic helicase, MDA-5, which was demonstrated in a mouse study.[82] However, mouse NK cells are now known to be differently regulated from human NK cells (e.g., presence of CD56 in human but not mouse NK cells).[96,97] Furthermore, some studies have implied that dsRNA provides a more amplified response through TLR3,[17] and TLR3$^{-/-}$ NK cells reportedly failed to respond to dsRNA stimulation.[20] For instance, treatment with 10 μg mL^{-1} of dsRNA resulted in almost 2.5-fold higher activation of TLR3 activation compared to that of MDA5.[17] In yet another study, MDA5 was shown to be dispensable for CD8^{+} T cell priming by Poly I:C.[98] Nevertheless, a limitation of this study is the lack of MDA5$^{-/-}$ cells which could have been studied in parallel to TLR3 expressing NK cells. Altogether, hiltonol administration in vivo may activate contractility via multiple PRRs in multiple immune cell types and together, upregulate anticancer activities. Future studies may be required to distinguish distinct and complementary roles of the various PRRs in response to hiltonol pretreatment in humans in vivo.

The interesting observation that higher dose of hiltonol (25 μg mL^{-1}) was unable to stimulate a robust enhancement of NK cell cytotoxicity led to two possible explanations. As demonstrated in Figure 3, ROS production was increased dose-dependently of Hiltonol. Hence, high ROS might induce oxidative stress to NK cells. To overcome this, the combinatorial treatment of NK cells with cytokines (e.g., IL15) with hiltonol may be explored. In one study, IL-15–primed NK cells showed a high content of the antioxidant scavenger, thioredoxin (Trx),[99] which indicates the regulation of ROS generated. Another possible explanation is feedback inhibition induced by hiltonol treatment. It is known that dsRNA stimulation on NK cells activate type 1 interferons. In one study, prolonged viral activation of NK cell type 1 interferon response was reported to result in immunosuppression through type 1 interferon receptors expressed on NK cells.[100] Hence, it may be a self-preservation mechanism by NK cells to prevent ROS-induced overactivation and premature exhaustion and ROS-cytotoxicity. On the other hand, the present study focused on the relationship between ERK and ROS. However, ROS is also well known to inhibit phosphatases[58,101] and the dephosphorylation of the SHP-1 tyrosine phosphatase in NK cells limits NK cytotoxicity.[102] Hence, high ROS levels may also concurrently elicit multiple side effects undesirable for NK activity.

In this study, we utilized various small molecule inhibitors to pharmacologically inhibit TAZ activity (verteporfin) and c-Myc (G3798) activity. The inhibition of c-Myc, a downstream target of the transcriptional coactivator TAZ, likewise enhanced the cytotoxicity of NK cells against the cancer cell lines studied. However, inhibition of c-Myc seemed to result in lesser cancer cell death (≈1.5-fold) compared to hiltonol treatment (≈2.0-fold). These observations again suggest that hiltonol inactivation of TAZ through RhoA-MLC2 and LATS1 activation may not be the only signaling axis. As suggested above, other pathways may be simultaneously activated by TLR3/MDA5 activation. On the other hand, our results vividly illustrate how the subcellular localization of two endogenous proteins, TAZ and Eomes, affects NK cytotoxicity, which could be potentiated by an exogenous chemical inhibitor of c-Myc, G3798. It would be pertinent in the future to test whether a cocktail of various inhibitors, activators, and neutralizing antibodies would further enhance NK cell cytotoxicity. Some of the options may include c-Myc inhibitor combined with verteporfin or hiltonol, and hiltonol combined with IL15 and other endogenous proteins such as TGFβ that activates NK contractility.[1] However, as mentioned in the previous paragraph, a note of caution is a possible increase in ROS generated by NK cells, to levels which may be self-cytotoxic. We showed that a high dosage of hiltonol (25 μg mL^{-1}) increased ROS production which reduced the enhanced NK cytotoxicity. A small amount of ROS was proficient in improving NK metabolism and function.[54,58,59] However, high ROS levels could be cytotoxic to NK cell itself. Furthermore, like most pharmacological inhibitors used at high dosage, the use of MEK/ERK1/2 inhibitor to limit ROS production in hNK cells may elicit off-target effects. Future experiments in vitro and in vivo with ERK1/2 knockout model cell lines or mice could shed light on whether ROS is specifically activated by ERK1/2 and vice versa. Nevertheless, our findings may perhaps explain why high doses of hiltonol/Poly-I:C were unable to sustain an increase in NK cell cytotoxicity in vitro and in vivo.[45–47,103]

Altogether, we have demonstrated a mechanistic understanding on how cell "force" (intracellular contractility) inactivates TAZ to promote NK cytotoxicity toward cancer cells. Our findings may provide an innovative avenue for ex vivo rejuvenation/activation of autologous NK cells for anticancer immunotherapies.

4. Experimental Section

Except for imaging flow cytometry, proximity ligation assay and DHE and MitoSOX assays, all other methodologies are adapted from the previous publication[1] with slight modifications. The resource table for antibodies and primers, and flow cytometry gating and controls used in this paper can be found in Tables S1 and S2 of the Supporting Information.

Cell Culture and Drug Treatments: Isolated primary hNK cells were expanded for one week before experiments following the manufacturer's recommendation. hNK was cultured in NK MACS medium (Miltenyi Biotec) supplemented with 1% NK MACS (Miltenyi Biotec), 5% human AB serum (Sigma-Aldrich), and 25 ng mL^{-1} IL-2 (Miltenyi Biotec). NCI-H1299, NCI-H1975, MCF7, MDA-MB-231, and K562 were obtained from the American Type Culture Collection. NK-92 cell line was maintained in RPMI 1640 supplemented with 12.5% FBS, 12.5% horse serum (Gibco), 1% penicillin/streptomycin, and supplemented with 10 ng mL^{-1} IL-2. For nonsmall cell lung cancer cells, NSCLCs (NCI-H1299 and NCI-H1975) and breast cancer cell lines (MCF7 and MDA-MB-231), TrypLE Select Enzyme (Gibco) was used for passaging cells. Only cells within passages 3 to 20 were used for experiments. All cell lines were supplemented with Plasmocin Prophylatic (Invivogen Cat# ant-mpp) for the prevention of mycoplasma contamination and routinely tested and verified to be free from mycoplasma using MycoStrip (Invivogen Cat # rep-mys) (Figure S8, Supporting Information). All cells were grown at 37 °C with 5% CO_2.

Poly:ICLC (Hiltonol) is a clinical grade formulation of poly-I:C stabilized with poly-L-lysine and carboxymethylcellulose manufactured by Oncovir. For drug treatments, cultured cells were treated with hiltonol (Oncovir Inc.), c-Myc inhibitor G3798 (Sigma-Aldrich, Cat# 10074-G5), verteporfin (Sigma-Aldrich, Cat#SML0534), and blebbistatin (Sigma-Aldrich, Cat#

203390) at indicated concentrations represented on the figures. 1× PBS and DMSO were used as vehicle controls for hiltonol, and G3798, verteporfin, and blebbistatin, respectively. The Rho activator CN03 was purchased from Cytoskeleton Inc. (Cat# CN-03) and diluted in sterile water.

Isolation of Peripheral Blood Mononuclear Cells (PBMCs) and Primary NK Cells: The protocols for isolation of PBMC from healthy donors were approved by the Health Sciences Authority Singapore (HSA) and the National University of Singapore Institutional Review Board (201706-06 and H-17-028E). Apheresis cones from healthy donors were obtained from the HSA. PBMCs were isolated from the blood samples using Ficoll-Paque (GE Healthcare, Cat# 17144003) and gradient centrifugation. The middle layers containing PBMCs were then enriched for primary hNK by negative selection using the EasySep Human NK Cell Enrichment Kit (StemCell Technologies, Cat# 19055), following the manufacturer's protocol. Isolated hNK cells are CD56+ and CD3− (Figure S8A, Supporting Information).

Coculture of NK Cell with Lung or Breast Cancer Cells: The effector (NK-92 or hNK) to target (cancer cells) was cocultured in a ratio of 2.5:1 as previously determined.[1,104] Briefly, hNK and NK-92 cells were prestained with CFSE (Sigma) according to the manufacturer's protocol, which was able to perpetuate stained cells for as long as 6 days as determined previously,[1] except for those used for cytotoxicity assay against model target cell line, K562. Lung and breast cancer cells were preseeded for at least 8 h for them to attach to cell culture plate. Coculture was carried out in NK MACS media supplemented with 25 ng mL^{-1} IL2 for hNK cells, or 10% RPMI supplemented with 10 ng mL^{-1} IL-2 for NK-92 cells.

NK Cell Cytotoxicity Assay against K562 Cells: The effector (NK-92 or hNK) to target (K562) was 5:1 and 1:1, respectively, as previously determined by the group.[1,104] Target cells were prestained with CFSE prior to coculture with NK cells for cytotoxicity assay. After a 4-h incubation period maintained at 37 °C with 5% CO_2, dead cells were stained with fixable viability dye eFluor506 (eBioscience, Cat# 65-0866-14) on ice for 30 min and immediately fixed with 2% PFA for analysis using flow cytometry. The gating strategy to identify CFSE-labeled dead K562 cells is in Figure S2 of the Supporting Information.

The Calcein-AM (Abcam, Cat# ab228556) release assay was performed according to the manufacturer's staining protocol. Briefly, target K562 cells were stained with Calcein-AM dye diluted in the dilution buffer (1:500) provided, and incubated for 30 min at 37 °C with 5% CO_2. The target cells were then washed once with RPMI media to remove any residual Calcein-AM dye. At least 3 wells were allocated for spontaneous cell death and maximum cell lysis was effected with 1% Triton-X in water, as controls. The effector (NK-92 or hNK) to target (Calcein-AM stained K562) ratio was 5:1 and 1:1, and after a 4-h incubation period, the supernatant was collected and measured for fluorescence signal at Ex/Em = 485/530 nm. The cytotoxicity percentage was obtained by reading the fluorescence values of [(NK + K562) − (Spontaneous K562)]/[(maximum cell lyse) − (spontaneous K562)].

Transfection and Transduction (siRNA and Lenti-Virus): NK cells were transfected with scrambled or ON-TARGET plus human WWTR1 SMARTpool siRNA from Dharmacon Inc, (CCGCAGGGCUCAUGAGUAU, GGACAAACACCCAUGAACA, AGGAACAAACGUUGACUUA, CCAAAUCUCGUGAUGAAUC) using the Neon Transfection System (Invitrogen) and according to the manufacturer recommended parameters. Following transfection, cells were allowed to recover in antibiotic-free media for 48 h.

The Lenti-ORF clone of Human WW domain containing transcription regulator 1 (WWTR1/TAZ), transcript variant 1, mGFP-tagged, in vector pLenti-C-mGFP-P2A-Puro was purchased from manufacturer, OriGene (Cat# RC231269L4). The manufacturer's protocol was used for viral production by mixing pLenti-C-TAZ-mGFP-P2A-Puro with packaging plasmids and transfection reagent from the Lenti-vpak packaging kit (OriGene, Cat#TR30037). The mixture was transfected into HEK293T cells to generate pseudoviral particles. NK-92 cells stably expressing TAZ-mGFP were established by transduction with pseudoviral particles with 8 μg mL^{-1} polybrene (Sigma-Aldrich, Cat# TR-1003-G). Stable cell lines were established through selection with puromycin (Sigma-Aldrich, Cat# P4512) and fluorescence-activated cell sorting.

Western Blot Analysis and Active RhoA Binding Assay: The Western blot procedures were performed, as previously described.[1] Briefly, cells were washed once with ice cold 1× PBS and lysed with ice cold RIPA supplemented with protease inhibitor, sodium orthovanadate, sodium fluoride, and β-Glycerophosphate. BCA assay was performed to prepare samples of equal protein concentration. 4× loading dye containing 2-Mercaptoethanol was added to the sample before boiling the sample at 85 °C for 10 min and ran on a denaturing SDS-PAGE gel. The results were visualized by ChemiDoc Touch (Bio-Rad) and analyzed using Image Lab V 5.2.1. The antibodies used are listed in Table S2 of the Supporting Information.

The Rhotekin-RBD Beads (Binds Active Rho Proteins) from Cytoskeleton Inc. (Cat#RT02) was used to pull down active RhoA-GTP in cell lysates. The procedures for pull down follow the manufacturer's protocol.

RT-qPCR Analysis: RNA extraction was carried out using Pure-NA Fast Total RNA extraction kit following the manufacturer's protocol. The cDNA across samples was generated from equal amounts of RNA using SuperScript IV VILO Master Mix following the manufacturer's protocol. Diluted cDNA (20 ng μL^{-1}) was used to quantify the delta Cq values of the samples using SsoFast EvaGreen Supermix from Biorad on the Bio-Rad CFX 96 Real-Time PCR Detection System.

Immunofluorescence and Microscopy: For immunofluorescence staining, cells were centrifuged at 500 × *g* for 5 min and fixed with 4% PFA for 15 min at 37 °C. Free aldehydes were quenched with freshly prepared sodium borohydride (0.01%; Sigma-Aldrich, Cat# 452882) dissolved in 1× PBS for 5 min. Samples were washed thrice with 1× PBS at 5 min intervals and 3% bovine serum albumin and 0.2% Triton X-100 in 1× PBS (blocking buffer) was used to permeabilize and block the samples. The appropriate primary antibodies were dissolved in blocking buffer following manufacturer's recommendation, and incubated for 45 min at room temperature. This was followed by washing thrice with 1× PBS and incubating with Goat anti-Rabbit IgG (H+L) Highly Cross-Adsorbed Secondary Antibody, Alexa Fluor – 647 conjugated secondary antibodies (ThermoFisher Scientific, Cat# A32733), and DAPI (ThermoFisher Scientific, Cat# D1306) diluted in 3% BSA in 1× PBS. Finally, the cells were washed thrice with 1× PBS and placed in an iBidi glass-bottom dish (iBidi, Cat# 81218-200) precoated with 0.01% poly-L-lysine (Invitrogen, Cat# P8920). The glass bottom dishes were centrifuged at 500 × *g* for 5 min using a swing-out bucket rotor. For visualization of actin, Alexa Fluor 488 Phalloidin (ThermoFisher Scientific, Cat# A12379) stain was used together with the secondary antibodies at 1:500 dilution.

Imaging was performed on a Yokogawa CSU-W1 (Nikon TiE system) spinning disk microscope using a 1.40 numerical aperture (NA) oil immersion 100× objective. For comparison between samples, the binning, laser powers, and exposure time were kept constant, and all samples were stained with a master mix of primary and secondary antibodies.

Laser Ablation of NK Cell Actin Filaments: The recoil velocity (measured by laser ablation) due to tensional release of actin network mesh within the cells is measured by monitoring distinctive features before, during and after UV laser ablation. Spatiotemporal information of the distinctive features after UV ablation was obtained and quantified using MTrackJ plugin in Fiji imageJ. Fitting of calculated distance between points of distinctive features was carried out using a linear function and a single exponential function, or a linear function and a double exponential function. The single exponential function was used for datasets with slow recoil velocity to obtain slow elastic response of the actin network mesh upon ablation. To obtain datasets with fast recoil velocity, double exponential function was used for fast elastic response of the actin network mesh upon ablation. Recoil velocity was calculated as the derivative of the abovementioned functions using methods mentioned in earlier literatures.[1,51,105]

The linear function is as follows

$$f\ (t) = p_1\, t + p_2 \tag{1}$$

where t is approximate time when UV laser shutter is opened, p_1 is deformation speed for linear model, and p_2 is the initial length between points of distinctive features at $t = 0$ s for linear model.

The single exponential model is as follows

$$f\ (t) = a + Ae^{\left(\frac{-1(t-b)}{\tau}\right)} \quad (2)$$

where t is approximate time when UV laser shutter is opened, a is the initial length between points of distinctive features at $t = 0$ s for exponential model, τ is ratio of Young's modulus to viscosity, and A and b are arbitrary constants.

The double exponential model is as follows

$$f\ (t) = a + A_1 e^{\left(\frac{-1(t-b)}{\tau_1}\right)} + A_2 e^{\left(\frac{-1(t-b)}{\tau_2}\right)} \quad (3)$$

where t is approximate time when UV laser shutter is opened, a is the initial length between points of distinctive features at $t = 0$ s for exponential model, τ_1 and τ_2 are ratios of Young's modulus to viscosity, and A_1, A_2, and b are arbitrary constants.

Preparation of Representative Videos for Laser Ablation of NK Cell Actin Filaments: Representative videos were edited for the following conditions:

NK92 control	hNK control	hNK with U0126
NK92 with 5 μg mL^{-1} hiltonol	hNK with 5 μg mL^{-1} hiltonol	hNK with U0126 and 5 μg mL^{-1} hiltonol
NK92 with 10 μg mL^{-1} hiltonol	hNK with 10 μg mL^{-1} hiltonol	hNK with U0126 and 10 μg mL^{-1} hiltonol

To analyze actin fluorescence intensities in representative videos, the built-in plugin LUT's Fire in ImageJ was used to pseudocolor the images. Next, the videos were cropped using a 150 by 150 pixel region of interest (ROI) to focus on the cells that underwent recoil measurement. Each cropped video contained a 5 μm scale-bar timer indicating the video's time interval of 1 s, and arrows marking the reference points used to obtain the recoil displacement. The videos to Audio Video Interleave format were then converted using Joint Photographic Experts Group compression with a play rate of 15 frames per second (fps).

Preparation of Hard and Soft PDMS Substrate for Traction Force Microscopy: PDMS gel was utilized as a substrate to create two levels of stiffness: soft (5.84 kPa) and hard (43.37 kPa). To achieve the desired stiffness, a mixture of CY52-276A and CY52-276B components (Dow Corning) was prepared in a 5:4 and 5:7 ratio, respectively, as described previously.[106] The mixed gel was then either spin-coated onto glass-bottom Petri dishes (IWAKI) at 1000 rpm for 1 min for imaging analysis or added into the wells of a 6-well plate for western analysis. Afterward, the mixed gel was cured at 80 °C for 2 h and treated with oxygen plasma to remove any organic and hydrocarbon material. This treatment exposed silanol (SiOH) groups on the PDMS surface, rendering it more hydrophilic and increasing surface wettability. Lastly, a fibronectin solution of 10 μg mL^{-1} was coated to the PDMS surface to activate it for cell attachment and adhesion.

Traction Force Microscopy and Quantification: TFM was used as a technique to measure local substrate deformations by imaging the displacements of fluorescent beads on the surface of a soft elastic gel.[107] PDMS gel was utilized to create a soft 15 kPa TFM substrate by preparing a mixture of CY52-276A and CY52-276B components (Dow Corning) at 1:1 ratio, as described by earlier works.[108,109] Approximately 40 μL volume of PDMS mixture was pipetted on each glass bottom dish (IBIDI) and spin-coated for 1 min at 1000 rpm before curing in 80 °C oven for 2 h. Next, PDMS surface was silanized with 5% 3-Aminopropyl)trimethoxysilane (Sigma A3648) diluted with absolute ethanol for 15 min before washing off with absolute ethanol and dried inside the 80 °C oven for 1 h. Fluorescent nanobead solution was prepared at 1:500 ratio with distilled water and carboxylate-modified microspheres of diameter 0.2 μm, dark red fluorescent (660/680 nm), 2% solids (Invitrogen). Bead solution was then poured onto the dish and incubated for 15 min before aspiration and further dried inside the 80 °C oven for 15 min. Lastly, the beads were passivated by adding 100 mM of Tris solution at pH 7.0 (Sigma-Aldrich) and incubated for 30 min. After incubation, Tris solution was aspirated and PDMS substrates were flooded with phosphate-buffered saline (1× PBS; Sigma-Aldrich) for storage in 4 °C.

The TFM substrates were coated with 10 μg mL^{-1} of fibronectin solution and incubated at 37 °C for at least 30 min prior to cell seeding. Cells and beads were imaged every 5 min using a spinning disk microscope. Particle image velocimetry and traction force analyses were performed using in-house code.

Flow Cytometry and Imaging Flow Cytometry: The antibodies used for flow cytometry analysis are represented in Table S2 of the Supporting Information and their respective FMO are represented in Figure S8B of the Supporting Information. For cell surface staining of receptors, fluorophore-conjugated antibodies were diluted in 1× PBS supplemented with 2% FBS at 1:100 dilution. NK cells were stained with the respective antibodies on ice for 10 min, followed by staining with fixable viability dye eFluor506 (eBioscience) on ice for 30 min. The cells were immediately sent for flow cytometry analysis to distinguish between live and dead cells and the expression of surface proteins.

To detect intracellular proteins, cells were first stained with fixable viability dye eFluor506 (eBioscience) on ice for 30 min and subsequently fixed with Intracellular Fixation and Permeabilization Buffer Set (eBioscience) for 40 min. Fixed cells were then stained for 30 min with the respective conjugated antibodies in permeabilization buffer at 1:100 dilution. Flow cytometry data were acquired using the CytoFLEX LX machine from Beckman Coulter, and all flow cytometry data were analyzed using FlowJo V10.4.

For imaging flow cytometry, samples were prepared according to the immunofluorescence staining methodology, to stain for DAPI and TAZ. Data were obtained using Amnis ImageStreamX Mark II Imaging Flow Cytometer. Fluid pressure was set to "low" for high sensitivity. The cells were gated sequentially for high HMG (better focus), single cells, DAPI-TAZ double-positive cells, and nuclear localization (high similarity dilate). The template was saved and used for analysis of different sample conditions. A single color control (DAPI or TAZ only) was used to automatically populate the compensation matrix. All data were analyzed with the IDEAS 6.0 software using the wizard for nuclear translocation. DAPI (Ch7) was used as nuclear probe and TAZ (Ch11) was used as the translocating probe. The gating strategy is represented in Figure S7 of the Supporting Information.

Proximity Ligation Assay: Proximity ligation assay experiments were carried out using Duolink flowPLA Detection Kit – FarRed (Sigma-Aldrich, # DUO94004) following the manufacturer's protocol. A sample with no primary antibodies but with the PLA probes was used as the technical negative control as recommended by the manufacturer. NK cells were fixed with warm 37 °C PFA for 15 min at room temperature (RT) and subsequently permeabilized with 0.2% Triton X-100. Afterward the samples were blocked with Duolink Blocking Solution and incubated with primary antibodies (mouse actin and rabbit LATS1 antibodies; Table S2, Supporting Information) for 1 h. The subsequent steps of the PLA followed the manufacturer's instructions. Data analysis of flow-cytometry PLA was performed using CytoFLEX LX machine from Beckman Coulter, and all flow cytometry data were analyzed using FlowJo V10.4.

DHE and MitoSOX Assay: The DHE assay kit for the measurement of intracellular superoxide and hydrogen peroxide was purchased from Abcam (Cat#ab236206). The MitoSOX for the measurement of mitochondria superoxide was purchased from ThermoFisher Scientific (Cat#M36008). The manufacturer's protocol was followed throughout. Antimycin A and N-Acetyl Cysteine Assay from the DHE assay kit were used as positive and negative controls, respectively. All cells were analyzed live and no fixation was involved in any step. Data acquisition of DHE and MitoSOX signals were performed using CytoFLEX LX machine measured in PE channel, and all flow cytometry data were analyzed using FlowJo V10.4.

Quantification of Nuclear-Cytoplasmic Ratio: Microscopy images obtained were analyzed using Image J V2.0. The nuclear/cytosolic ratio was analyzed as previously described[1,34] with slight modifications to accommodate the smaller cytoplasmic areas in NK cells. A Z-stacked image (step size 0.2 μm) encompassing the whole cell was obtained and the stacks demarcated by nuclear DAPI staining were Z-stacked for quantification of nuclear/cytoplasmic ratio. The DIC image, DAPI, and antibody channels were then merged to demarcate, respectively, the cell cytoplasm (CFSE

and DIC areas without DAPI stain) and the nucleus (DAPI) and TAZ. To avoid measurement of an ROI in the nucleus that exceeded the cytoplasmic ROI, the biggest possible ROI drawn in the cytosol next to the DAPI-stained nucleus was first measured. The same ROI was then shifted inside the nucleus to measure the mean intensity of TAZ within the nucleus. The nuclear-cytoplasmic ratio was derived by dividing the nuclear intensity by cytosol intensity.

Analysis of NK Cell Nuclear Size and Perimeter: To analyze the geometric properties of the nuclei of NK cells, DAPI-stained nuclei images were first segmented from the stack images before summing the z-projected slices to convert the *x-y-z* images into *x-y* images. To remove and blur out the speckled features within the nuclei, images were filtered with Gaussian Blur. Next, nuclei objects were separated from the background through adjusting the threshold to obtain the images in black and white (0–255). To separate nuclei touching each other, Watershed function built-in in ImageJ was utilized to find the center of each nuclei object, distance map from nuclei object center points to edges of nuclei objects calculated, then a topological map was formed with lines created to separated nuclei touching one another. Once images were processed, Analyze Particles built-in function in ImageJ was used to locate the nuclei objects, count them, and obtain statistical parameters (e.g., perimeter of nucleus, area of nucleus) from the ROI demarcating each nucleus. Incomplete nuclei on the edges of the image were excluded.

Statistical Analysis: All graphs are represented as mean ± SEM. Statistical analysis was carried out using Prism 8.2.1 (GraphPad Software). For statistical significance, *p*-value < 0.05 is considered as significant (*$p < 0.05$, **$p < 0.01$, ***$p < 0.001$, ****$p < 0.000$). The Wilcoxon rank sum test (also known as Mann–Whitney U test) and Kruskal–Wallis test were used for statistical analyses of fold changes. The unpaired Student's *t*-test was used to compare other analyses requiring comparison between two groups. For all experiments, donor hNK cells isolated from at least three different PBMCs were used. At least three replicates were performed with all other cell lines used in this paper.

Data and Materials Availability: All data needed to evaluate the conclusions of the paper are present in the paper and/or the Supporting Information. Additional data and codes related to this paper may be requested from the authors upon reasonable request.

Supporting Information

Supporting Information is available from the Wiley Online Library or from the author.

Acknowledgements

This project is supported by the National Research Foundation, Singapore under its RIE Roles for SGUnited Jobs - NUS Tranche 1 Project (NRF-MP-2020-0004), Administered in NUS under the NUS Resilience and Growth Postdoctoral Fellowship. The authors thank the core facilities of the National University of Singapore, Department of Biological Sciences (NUS-DBS), Confocal Microscopy Unit and Flow Cytometry Laboratory (NUS-CMA), Department of Microbiology (NUS-Microbiology) and Mechanobiology Institute of Singapore, and Centre for BioImaging Sciences (NUS-MBI) for technical support. The authors thank Dongxue Hu for advice on DHE and MitoSOX assays. The illustrations were created with BioRender.

Conflict of Interest

A.M.S. is an employee of Oncovir Inc, which produces Hiltonol. All other authors declare no conflict of interest.

Author Contributions

D.C.P.W., Y.-C.L., B.C.L., and J.L.D. contributed equally to this work. Y.-C.L, and B.C.L. share senior author ship. D.W.C.P., Z.X., N.S., I.Y., T.T., and J.Y.Y. conducted the experiments. A.M.S. provided hiltonol and background information. Y.-C.L., B.C.L., and J.L.D. provided advice and samples or reagents. D.C.P.W. and J.L.D. designed the experiments and wrote the manuscript. All authors commented on the manuscript.

Data Availability Statement

The data that support the findings of this study are available from the corresponding author upon reasonable request.

Keywords

dsRNA-induced intracellular contractility, LATS, mechanobiology, natural killer cell cytotoxicity, TAZ

Received: January 12, 2023
Revised: April 10, 2023
Published online:

[1] D. C. P. Wong, E. H. C. Lee, J. Er, I. Yow, R. A. G. Koean, O. Ang, J. Xiao, B. C. Low, J. L. Ding, *Front. Cell Dev. Biol.* **2022**, *10*, 871326.
[2] E. H. C. Lee, D. C. P. Wong, J. L. Ding, *Front. Immunol.* **2021**, *12*, 734551.
[3] L. M. McLane, S. F. Ngiow, Z. Chen, J. Attanasio, S. Manne, G. Ruthel, J. E. Wu, R. P. Staupe, W. Xu, R. K. Amaravadi, X. Xu, G. C. Karakousis, T. C. Mitchell, L. M. Schuchter, A. C. Huang, B. D. Freedman, M. R. Betts, E. J. Wherry, *Cell Rep.* **2021**, *35*, 109120.
[4] J. Bi, X. Wang, *Front. Immunol.* **2020**, *11*, 1945.
[5] J. Y. Noh, S. R. Yoon, T. D. Kim, I. Choi, H. Jung, *J. Immunol. Res.* **2020**, *2020*, 2045860.
[6] M. Adib-Conquy, D. Scott-Algara, J. M. Cavaillon, F. Souza-Fonseca-Guimaraes, *Immunol. Cell Biol.* **2014**, *92*, 256.
[7] K. N. Schmidt, B. Leung, M. Kwong, K. A. Zarember, S. Satyal, T. A. Navas, F. Wang, P. J. Godowski, *J. Immunol.* **2004**, *172*, 138.
[8] C. Guillerey, M. T. Chow, K. Miles, S. Olver, J. Sceneay, K. Takeda, A. Möller, M. J. Smyth, *Oncoimmunology* **2015**, *4*, 1027468.
[9] H. Harjunpää, C. Guillerey, *Clin. Exp. Immunol.* **2020**, *200*, 108.
[10] J. Bi, Z. Tian, *Front. Immunol.* **2017**, *8*, 760.
[11] G. Santoni, C. Amantini, M. Santoni, F. Maggi, M. B. Morelli, A. Santoni, *Front. Immunol.* **2021**, *12*, 688918.
[12] D. Friedman, P. Simmonds, A. Hale, L. Bere, N. W. Hodson, M. R. H. White, D. M. Davis, *J. Cell Sci.* **2021**, *134*, jcs258570.
[13] L. Mordechay, G. L.e Saux, A. Edri, U. Hadad, A. Porgador, M. Schvartzman, *ACS Biomater. Sci. Eng.* **2021**, *7*, 122.
[14] W. Xu, R. Mezencev, B. Kim, L. Wang, J. McDonald, T. Sulchek, *PLoS One* **2012**, *7*, e46609.
[15] K. Hayashi, M. Iwata, *J. Mech. Behav. Biomed. Mater.* **2015**, *49*, 105.
[16] H. Sultan, A. M. Salazar, E. Celis, *Semin. Immunol.* **2020**, *49*, 101414.
[17] I. Perrot, F. Deauvieau, C. Massacrier, N. Hughes, P. Garrone, I. Durand, O. Demaria, N. Viaud, L. Gauthier, M. Blery, N. Bonnefoy-Berard, Y. Morel, J. Tschopp, L. Alexopoulou, G. Trinchieri, C. Paturel, C. Caux, *J. Immunol.* **2010**, *185*, 2080.
[18] P. R. Cooper, R. Lamb, N. D. Day, P. J. Branigan, R. Kajekar, L. San Mateo, P. J. Hornby, R. A. Panettieri, *Am. J. Physiol.: Lung Cell. Mol. Physiol.* **2009**, *297*, L530.
[19] K. Tewari, B. J. Flynn, S. B. Boscardin, K. Kastenmueller, A. M. Salazar, C. A. Anderson, V. Soundarapandian, A. Ahumada, T. Keler, S. L. Hoffman, M. C. Nussenzweig, R. M. Steinman, R. A. Seder, *Vaccine* **2010**, *28*, 7256.
[20] M. Matsumoto, M. Tatematsu, F. Nishikawa, M. Azuma, N. Ishii, A. Morii-Sakai, H. Shime, T. Seya, *Nat. Commun.* **2015**, *6*, 6280.

[21] J. H. Boyd, S. Mathur, Y. Wang, R. M. Bateman, K. R. Walley, *Cardiovasc. Res.* **2006**, *72*, 384.
[22] T. Hardigan, K. Spitler, T. Matsumoto, M. A. Carrillo-Sepulveda, *Pflugers Arch. Eur. J. Physiol.* **2015**, *467*, 2375.
[23] O. Matalon, A. Ben-Shmuel, J. Kivelevitz, B. Sabag, S. Fried, N. Joseph, E. Noy, G. Biber, M. Barda-Saad, *EMBO J.* **2018**, *37*, 96264.
[24] A. F. Carisey, E. M. Mace, M. B. Saeed, D. M. Davis, J. S. Orange, *Curr. Biol.* **2018**, *28*, 489.
[25] K. Krzewski, X. Chen, J. S. Orange, J. L. Strominger, *J. Cell Biol.* **2006**, *173*, 121.
[26] A. Al Absi, H. Wurzer, C. Guerin, C. Hoffmann, F. Moreau, X. Mao, J. Brown-Clay, R. Petrolli, C. P. Casellas, M. Dieterle, J. P. Thiery, S. Chouaib, G. Berchem, B. Janji, C. Thomas, *Cancer Res.* **2018**, *78*, 5631.
[27] D. C. P. Wong, J. L. Ding, *Biochim. Biophys. Acta, Rev. Cancer* **2023**, *1878*, 188860.
[28] A. Ben-Shmuel, B. Sabag, G. Biber, M. Barda-Saad, *Front. Cell Dev. Biol.* **2021**, *9*, 609532.
[29] S. Piccolo, S. Dupont, M. Cordenonsi, *Physiol. Rev.* **2014**, *94*, 1287.
[30] T. Panciera, L. Azzolin, M. Cordenonsi, S. Piccolo, *Nat. Rev. Mol. Cell Biol.* **2017**, *18*, 758.
[31] B. C. Low, C. Q. Pan, G. V. Shivashankar, A. Bershadsky, M. Sudol, M. Sheetz, *FEBS Lett.* **2014**, *588*, 2663.
[32] B. Zhao, L. Li, Q. Lei, K. L. Guan, *Genes Dev.* **2010**, *24*, 862.
[33] L. Hong, X. Li, D. Zhou, J. Geng, L. Chen, *Cell. Mol. Immunol.* **2018**, *15*, 1003.
[34] A. Elosegui-Artola, I. Andreu, A. E. M. Beedle, A. Lezamiz, M. Uroz, A. J. Kosmalska, R. Oria, J. Z. Kechagia, P. Rico-Lastres, A. L. Le Roux, C. M. Shanahan, X. Trepat, D. Navajas, S. Garcia-Manyes, P. Roca-Cusachs, *Cell* **2017**, *171*, 1397.
[35] E. Stampouloglou, N. Cheng, A. Federico, E. Slaby, S. Monti, G. L. Szeto, X. Varelas, *PLoS Biol.* **2020**, *18*, e3000591.
[36] K. P. Meng, F. S. Majedi, T. J. Thauland, M. J. Butte, *J. Exp. Med.* **2020**, *217*, e20200053.
[37] H. Wang, S. Zhang, Y. Zhang, J. Jia, J. Wang, X. Liu, J. Zhang, X. Song, S. Ribback, A. Cigliano, M. Evert, B. Liang, H. Wu, D. F. Calvisi, Y. Zeng, X. Chen, *J. Hepatol.* **2022**, *76*, 123.
[38] G. Monaco, B. Lee, W. Xu, S. Mustafah, Y. Y. Hwang, C. Carré, N. Burdin, L. Visan, M. Ceccarelli, M. Poidinger, A. Zippelius, J. Pedro de Magalhães, A. Larbi, *Cell Rep.* **2019**, *26*, 1627.
[39] J. E. D. Thaventhiran, A. Hoffmann, L. Magiera, M. De La Roche, H. Lingel, M. Brunner-Weinzierl, D. T. Fearon, *Proc. Natl. Acad. Sci. USA* **2012**, *109*, E2223.
[40] S. Kurtulus, K. Sakuishi, S. F. Ngiow, N. Joller, D. J. Tan, M. W. L. Teng, M. J. Smyth, V. K. Kuchroo, A. C. Anderson, *J. Clin. Invest.* **2015**, *125*, 4053.
[41] S. Sivori, M. Falco, M. D. Chiesa, S. Carlomagno, M. Vitale, L. Moretta, A. Moretta, *Proc. Natl. Acad. Sci. USA* **2004**, *101*, 10116.
[42] Y. Lu, T. Wu, O. Gutman, H. Lu, Q. Zhou, Y. I. Henis, K. Luo, *Nat. Cell Biol.* **2020**, *22*, 453.
[43] H. Qu, D. Qi, X. Wang, Y. Dong, Q. Jin, J. Wei, C. Quan, *Int. J. Mol. Sci.* **2022**, *23*, 129.
[44] L. H. Glimcher, M. J. Townsend, B. M. Sullivan, G. M. Lord, *Nat. Rev. Immunol.* **2004**, *4*, 900.
[45] S. C. Chang, J. L. Ding, *Cell Death Differ.* **2014**, *21*, 1388.
[46] W. H. Lau, X. G. Zhu, S. W. T. Ho, S. C. Chang, J. L. Ding, *OncoTargets Ther.* **2017**, *8*, 32884.
[47] S. C. Chang, B. X. Zhang, E. C. Y. Su, W. C. Wu, T. H. Hsieh, A. M. Salazar, Y. K. Lin, J. L. Ding, *Int. J. Mol. Sci.* **2021**, *22*, 1626.
[48] N. C. Stowell, J. Seideman, H. A. Raymond, K. A. Smalley, R. J. Lamb, D. D. Egenolf, P. J. Bugelski, L. A. Murray, P. A. Marsters, R. A. Bunting, R. A. Flavell, L. Alexopoulou, L. R. San Mateo, D. E. Griswold, R. T. Sarisky, M. L. Mbow, A. M. Das, *Respir. Res.* **2009**, *10*, 43.
[49] S. Pisegna, G. Pirozzi, M. Piccoli, L. Frati, A. Santoni, G. Palmieri, *Blood* **2004**, *104*, 4157.
[50] J. Zhang, F. Alisafaei, M. Nikolić, X. A. Nou, H. Kim, V. B. Shenoy, G. Scarcelli, *Small* **2020**, *16*, e1907688.
[51] Y. Hara, M. Shagirov, Y. Toyama, *Curr. Biol.* **2016**, *26*, 2388.
[52] Z. M. Goeckeler, R. B. Wysolmerski, *J. Cell Biol.* **1995**, *130*, 613.
[53] J. Liu, S. Liu, M. Xia, S. Xu, C. Wang, Y. Bao, M. Jiang, Y. Wu, T. Xu, X. Cao, *Proc. Natl. Acad. Sci. USA* **2013**, *110*, 7814.
[54] Y. Son, Y.-K. Cheong, N.-H. Kim, H.-T. Chung, D. G. Kang, H.-O. Pae, *J. Signal Transduction* **2011**, *2011*, 792639.
[55] T. Verfaillie, N. Rubio, A. D. Garg, G. Bultynck, R. Rizzuto, J. P. Decuypere, J. Piette, C. Linehan, S. Gupta, A. Samali, P. Agostinis, *Cell Death Differ.* **2012**, *19*, 1880.
[56] L. Monturiol-Gross, M. Flores-Díaz, M. J. Pineda-Padilla, A. C. Castro-Castro, A. Alape-Giron, *PLoS One* **2014**, *9*, e86475.
[57] Z. Han, Y. Zhang, C. Wang, X. Liu, A. Jiang, Z. Liu, J. Wang, Z. Yang, Z. Wei, *J. Agric. Food Chem.* **2019**, *67*, 11230.
[58] S.-H. Lee, S. Almutairi, A. K. Ali, *J. Immunol.* **2017**, *198*, 222.20.
[59] A. Kotsafti, M. Scarpa, I. Castagliuolo, M. Scarpa, *Cancers* **2020**, *12*, 1748.
[60] A. K. Duwe, J. Werkmeister, J. C. Roder, R. Lauzon, U. Payne, *J. Immunol.* **1985**, *134*, 2637.
[61] D. C. P. Wong, J. Xiao, T. W. Chew, M. Pan, C. J. M. Lee, J. Ang, N. J. W. Lee, R. S.-Y. Foo, P. Kanchanawong, B. C. Low, *SSRN Electron. J.* **2021**, *9*.
[62] K. T. Furukawa, K. Yamashita, N. Sakurai, S. Ohno, *Cell Rep.* **2017**, *20*, 1435.
[63] I. Virtanen, J. Ylänne, T. Vartio, E. Saksela, *Scand. J. Immunol.* **1991**, *33*, 421.
[64] K. Somersalo, E. Saksela, *Eur. J. Immunol.* **1991**, *21*, 35.
[65] S. Visser-Grieve, Z. Zhou, Y. M. She, H. Huang, T. D. Cyr, T. Xu, X. Yang, *Cell Res.* **2011**, *21*, 1513.
[66] F. X. Yu, B. Zhao, N. Panupinthu, J. L. Jewell, I. Lian, L. H. Wang, J. Zhao, H. Yuan, K. Tumaneng, H. Li, X. D. Fu, G. B. Mills, K. L. Guan, *Cell* **2012**, *150*, 780.
[67] M. S. Alam, *Methods Mol. Biol.* **2022**, *2422*, 191.
[68] F. R. Mariotti, S. Petrini, T. Ingegnere, N. Tumino, F. Besi, F. Scordamaglia, E. Munari, S. Pesce, E. Marcenaro, A. Moretta, P. Vacca, L. Moretta, *Oncoimmunology* **2019**, *8*, e1557030.
[69] C. Wang, X. Zhu, W. Feng, Y. Yu, K. Jeong, W. Guo, Y. Lu, G. B. Mills, *Am. J. Cancer Res.* **2016**, *6*, 27.
[70] C. Wei, X. Li, *BMC Cancer* **2020**, *20*, 1042.
[71] J. Giraud, S. Molina-Castro, L. Seeneevassen, E. Sifré, J. Izotte, C. Tiffon, C. Staedel, H. Boeuf, S. Fernandez, P. Barthelemy, F. Megraud, P. Lehours, P. Dubus, C. Varon, *Int. J. Cancer* **2020**, *146*, 2255.
[72] P. Fusco, E. Mattiuzzo, C. Frasson, G. Viola, E. Cimetta, M. R. Esposito, G. P. Tonini, *Eur. J. Pharmacol.* **2021**, *893*, 173829.
[73] E. J. Lee, E. Seo, J. W. Kim, S. A. Nam, J. Y. Lee, J. Jun, S. Oh, M. Park, E. H. Jho, K. H. Yoo, J. H. Park, Y. K. Kim, *Proc. Natl. Acad. Sci. USA* **2020**, *117*, 29001.
[74] D. C. P. Wong, J. Xiao, T. W. Chew, M. Pan, C. J. M. Lee, J. W. Ang, I. Yow, T. Thivakar, M. Ackers-Johnson, N. J. W. Lee, R. S. Y. Foo, P. Kanchanawong, B. C. Low, *Adv. Sci.* **2022**, *9*, 1.
[75] F. Cichocki, R. J. Hanson, T. Lenvik, M. Pitt, V. McCullar, H. Li, S. K. Anderson, J. S. Miller, *Blood* **2009**, *113*, 3245.
[76] K. A. O. Martins, S. Bavari, A. M. Salazar, *Expert Rev. Vaccines* **2015**, *14*, 447.
[77] S. Y. Al Omar, E. Marshall, D. Middleton, S. E. Christmas, *Immunology* **2011**, *133*, 94.
[78] D. V. Rozanov, N. D. Rozanov, K. E. Chiotti, A. Reddy, P. A. Wilmarth, L. L. David, S. W. Cha, S. Woo, P. Pevzner, V. Bafna, G. G. Burrows, J. K. Rantala, T. Levin, P. Anur, K. Johnson-Camacho, S. Tabatabaei, D. J. Munson, T. C. Bruno, J. E. Slansky, J. W. Kappler, N. Hirano, S.

Boegel, B. A. Fox, C. Egelston, D. L. Simons, G. Jimenez, P. P. Lee, J. W. Gray, P. T. Spellman, *J. Proteomics* **2018**, *176*, 13.
[79] V. Llombart, M. R. Mansour, *EBioMedicine* **2022**, *75*, 103756.
[80] H. Han, A. D. Jain, M. I. Truica, J. Izquierdo-Ferrer, J. F. Anker, B. Lysy, V. Sagar, Y. Luan, Z. R. Chalmers, K. Unno, H. Mok, R. Vatapalli, Y. A. Yoo, Y. Rodriguez, I. Kandela, J. B. Parker, D. Chakravarti, R. K. Mishra, G. E. Schiltz, S. A. Abdulkadir, *Cancer Cell* **2019**, *36*, 483.
[81] T. Miyake, Y. Kumagai, H. Kato, Z. Guo, K. Matsushita, T. Satoh, T. Kawagoe, H. Kumar, M. H. Jang, T. Kawai, T. Tani, O. Takeuchi, S. Akira, *J. Immunol.* **2009**, *183*, 2522.
[82] S. McCartney, W. Vermi, S. Gilfillan, M. Cella, T. L. Murphy, R. D. Schreiber, K. M. Murphy, M. Colonna, *J. Exp. Med.* **2009**, *206*, 2967.
[83] C. T. T. Le, S. Y. Ahn, S. M. Kang, E. J. Ko, *Vaccines* **2021**, *9*, 1061.
[84] A. Lebid, L. Chung, D. M. Pardoll, F. Pan, *Front. Immunol.* **2020**, *11*, 580.
[85] H. Zhang, A. Schaefer, Y. Wang, R. G. Hodge, D. R. Blake, J. N. Diehl, A. G. Papageorge, M. D. Stachler, J. Liao, J. Zhou, Z. Wu, F. G. Akarca, L. K. de Klerk, S. Derks, M. Pierobon, K. A. Hoadley, T. C. Wang, G. Church, K. K. Wong, E. F. Petricoin, A. D. Cox, D. R. Lowy, C. J. Der, A. J. Bass, *Cancer Discovery* **2020**, *10*, 288.
[86] T. D. Pollard, *Cold Spring Harbor Perspect. Biol.* **2016**, *8*, a018226.
[87] N. Kastan, K. Gnedeva, T. Alisch, A. A. Petelski, D. J. Huggins, J. Chiaravalli, A. Aharanov, A. Shakked, E. Tzahor, A. Nagiel, N. Segil, A. J. Hudspeth, *Nat. Commun.* **2021**, *12*, 3100.
[88] A. Aihara, T. Iwawaki, N. Abe-Fukasawa, K. Otsuka, K. Saruhashi, T. Mikashima, T. Nishino, *J. Biol. Chem.* **2022**, *298*, 101779.
[89] X. Dai, P. She, F. Chi, Y. Feng, H. Liu, D. Jin, Y. Zhao, X. Guo, D. Jiang, K. L. Guan, T. P. Zhong, B. Zhao, *J. Biol. Chem.* **2013**, *288*, 34041.
[90] S. Mana-Capelli, D. McCollum, *J. Biol. Chem.* **2018**, *293*, 18230.
[91] S. Mana-Capelli, M. Paramasivam, S. Dutta, D. McCollum, *Mol. Biol. Cell* **2014**, *25*, 1676.
[92] M. Manukyan, P. Nalbant, S. Luxen, K. M. Hahn, U. G. Knaus, *J. Immunol.* **2009**, *182*, 3522.
[93] S. Koike, K. Yamasaki, T. Yamauchi, R. Shimada-Omori, K. Tsuchiyama, H. Ando, S. Aiba, *J. Dermatol. Sci.* **2019**, *96*, 168.
[94] M. T. Schreiber, B. Schuler, L. Li, D. J. Hall, *Innate Immun.* **2013**, *19*, 278.
[95] N. C. Bosch, R. E. Voll, C. J. Voskens, S. Gross, B. Seliger, G. Schuler, N. Schaft, J. Dörrie, *Ther. Adv. Med. Oncol.* **2019**, *11*, 1758835919891622.
[96] C. M. Sungur, W. J. Murphy, *Hematol. Am. Soc. Hematol. Educ. Program* **2013**, *2013*, 227.
[97] F. Colucci, J. P. Di Santo, P. J. Leibson, *Nat. Immunol.* **2002**, *3*, 807.
[98] Y. Wang, M. Cella, S. Gilfillan, M. Colonna, *J. Immunol.* **2010**, *184*, 2751.
[99] J. F. Collet, J. Messens, *Antioxid. Redox Signaling* **2010**, *13*, 1205.
[100] A. J. Lee, F. Mian, S. M. Poznanski, M. Stackaruk, T. Chan, M. V. Chew, A. A. Ashkar, *Front. Immunol.* **2019**, *10*, 1261.
[101] F. G. Meng, Z. Y. Zhang, *Biochim. Biophys. Acta, Proteins Proteomics* **2013**, *1834*, 464.
[102] A. Ben-Shmuel, B. Sabag, A. Puthenveetil, G. Biber, M. Levy, T. Jubany, F. Awwad, R. K. Roy, N. Joseph, O. Matalon, J. Kivelevitz, M. Barda-Saad, *eLife* **2022**, *11*, e73282.
[103] A. M. Salazar, R. B. Erlich, A. Mark, N. Bhardwaj, R. B. Herberman, *Cancer Immunol. Res.* **2014**, *2*, 720.
[104] R. Verma, J. Z. Er, R. W. Pu, J. Sheik Mohamed, R. A. Soo, H. M. Muthiah, J. K. C. Tam, J. L. Ding, *Front. Immunol.* **2020**, *11*, 1190.
[105] E. Meijering, O. Dzyubachyk, I. Smal, *Methods Enzymol.* **2012**, *504*, 183.
[106] Y. Zhang, X. Yang, C. Xiong, *Acta Mech. Sin.* **2021**, *37*, 554.
[107] S. R. K. Vedula, H. Hirata, M. H. Nai, A. Brugués, Y. Toyama, X. Trepat, C. T. Lim, B. Ladoux, *Nat. Mater.* **2014**, *13*, 87.
[108] T. Kawaue, I. Yow, Y. Pan, A. P. Le, Y. Lou, M. Loberas, M. Shagirov, X. Teng, J. Prost, T. Hiraiwa, B. Ladoux, Y. Toyama, *Dev. Cell* **2023**, *58*, 267.
[109] Y. Lou, T. Kawaue, I. Yow, Y. Toyama, J. Prost, T. Hiraiwa, *Biomech. Model. Mechanobiol.* **2022**, *21*, 1511.